

TUNING OF THE PHOTOLUMINESCENCE OF ELECTRON  
IRRADIATED MONOLAYER MoS<sub>2</sub> VIA LASER EXPOSURE



A Thesis Submitted in Partial Fulfillment of the Requirement for the  
Degree of Doctor of Philosophy in Physics  
Suranaree University of Technology  
Academic Year 2022

การปรับแต่งสภาพการเรืองแสงของโพลีบดินน์ไมด์ซัลไฟด์  
ชั้นเดียวที่ถูกอาบด้วยอิเล็กตรอนด้วยการฉายแสงเลเซอร์



นางสาวอิศรา ราศรีทัศน์

วิทยานิพนธ์นี้เป็นส่วนหนึ่งของการศึกษาตามหลักสูตรปริญญาวิทยาศาสตรดุษฎีบัณฑิต

สาขาวิชาฟิสิกส์

มหาวิทยาลัยเทคโนโลยีสุรนารี

ปีการศึกษา 2565

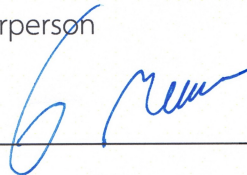
TUNING OF THE PHOTOLUMINESCENCE OF ELECTRON IRRADIATED  
MONOLAYER MoS<sub>2</sub> VIA LASER EXPOSURE

Suranaree University of Technology has approved this thesis submitted in  
partial fulfillment of the requirements for the Degree of Doctor of Philosophy.

Thesis Examining Committee



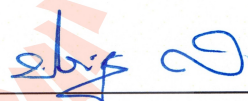
(Assoc. Prof. Dr. Panomsak Meemon)  
Chairperson



(Assoc. Prof. Dr. Worawat Meevasana)  
Member (Thesis Advisor)



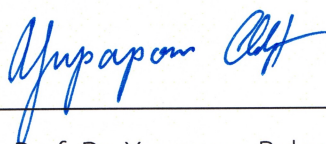
(Dr. Sorawis Sangtawesin)  
Member (Thesis Co-Advisor)



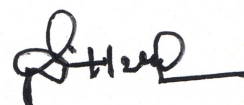
(Assoc. Prof. Dr. Prayoon Songsiriritthigul)  
Member



(Asst. Prof. Dr. Sukrit Sucharitakul)  
Member



(Assoc. Prof. Dr. Yupaporn Ruksakulpiwat)  
Vice Rector for Academic Affairs  
and Quality Assurance



(Prof. Dr. Santi Maensiri)  
Dean of Institute of Science



อิศรา ราศรีทัศน์ : การปรับแต่งสภาพการเรืองแสงของโมลิบดีนัมไดซัลไฟด์ชั้นเดี่ยวที่ถูกอบด้วยอิเล็กตรอนโดยการฉายแสงเลเซอร์ (TUNING OF THE PHOTOLUMINESCENCE OF ELECTRON IRRADIATED MONOLAYER MoS<sub>2</sub> VIA LASER EXPOSURE)

อาจารย์ที่ปรึกษา : รองศาสตราจารย์ ดร.วรวัฒน์ มีวาสนา, 65 หน้า.

คำสำคัญ: โมลิบดีนัมไดซัลไฟด์ชั้นเดี่ยว, การเรืองแสง, การฉายอิเล็กตรอน

ฟิล์มบางชั้นเดี่ยวของโมลิบดีนัมไดซัลไฟด์เป็นวัสดุที่มีความน่าสนใจเป็นอย่างมากและสามารถนำมาประยุกต์ใช้ในระบบเซ็นเซอร์แสงและอุปกรณ์อิเล็กทรอนิกส์เชิงแสงได้ ในงานวิจัยนี้ได้นำเสนอการปรับปรุงพื้นผิวของตัวอย่างโดยการฉายอิเล็กตรอนด้วยกล้องจุลทรรศน์อิเล็กตรอนแบบส่องกราดที่พลังงานต่ำ พบว่าสเปกตรัมของรามานหลังจากการฉายอิเล็กตรอนเคลื่อนไปหาความถี่ที่สูงขึ้นบ่งบอกถึงการมีออกซิเจนในอากาศมาเกาะบนพื้นผิว นอกจากนี้ยังมีปรากฏการณ์ที่น่าสนใจคือหลังจากการฉายด้วยเลเซอร์ที่มีความยาวคลื่น 532 นาโนเมตร การเรืองแสงจะลดลงและสามารถคืนตัวได้เมื่อเก็บไว้ในอากาศ โดยเราสามารถอธิบายกระบวนการคืนตัวของ การเรืองแสงได้จากสเปกตรัมของแสงหลังฉายเลเซอร์ พบว่ามีจำนวนของไดรอนเพิ่มขึ้นและจะลดลงเมื่อเก็บไว้ในอากาศ นอกจากนี้ยังพบว่า การลดลงของการเรืองแสงไม่สามารถกลับคืนมาได้ ในบรรยากาศของไนโตรเจนเพียงอย่างเดียว ดังนั้นจึงสรุปได้ว่าปรากฏการณ์ที่เกิดขึ้นเกิดจากออกซิเจนในอากาศมายึดเกาะบนพื้นผิวและทำการดึงอิเล็กตรอนออกมาจากระบบ ปรากฏการณ์การเปลี่ยนแปลงการเรืองแสงของสารได้โดยยิงแสงเลเซอร์ลงบนตัวอย่างที่มีการปรับปรุงพื้นผิวด้วยการฉายอิเล็กตรอนนี้ สามารถนำไปประยุกต์ใช้ระบบเซ็นเซอร์ก๊าซและอุปกรณ์อิเล็กทรอนิกส์เชิงแสงได้

สาขาวิชาฟิสิกส์

ปีการศึกษา 2565

ลายมือชื่อนักศึกษา

ลายมือชื่ออาจารย์ที่ปรึกษา

ลายมือชื่ออาจารย์ที่ปรึกษาร่วม

มหาวิทยาลัยเทคโนโลยีสุรนารี

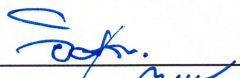
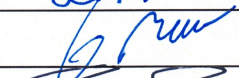



AISSARA RASRITAT : TUNING OF THE PHOTOLUMINESCENCE OF ELECTRON IRRADIATED MONOLAYER MoS<sub>2</sub> VIA LASER EXPOSURE. THESIS ADVISOR : ASSOC. PROF. WORAWAT MEEVASANA, Ph.D. 65 PP.

Keyword: MONOLAYER MoS<sub>2</sub>, PHOTOLUMINESCENCE, ELECTRON IRRADIATION

A monolayer of MoS<sub>2</sub> is a two-dimensional material that has attracted considerable attention in recent years due to its potential application in electrical and optoelectronic devices. Here, we report the photoluminescence intensity as a function of time from monolayer of MoS<sub>2</sub> that the surface modification via electron irradiation at low accelerating voltages. After electron irradiation, Raman spectra shifted to a higher frequency, indicating the presence of oxygen adsorption from the air onto the surface. Moreover, when the sample is exposed to a 532 nm excitation, the photoluminescence (PL) intensity decreases (i.e. quenches) and interestingly, it the intensity could be recovered when left in the dark for several hours, indicating it is not a permanent photobleaching. The PL spectra analysis of the modified monolayer MoS<sub>2</sub> shows increased trion state after exposure and reduced when kept in ambient condition. Additionally, the quenching process is irreversible when the experiment is repeated in the nitrogen atmosphere. It is consistent with oxygen adsorption onto the surface and the O<sub>2</sub> molecules subsequently deplete electrons from the sample. Our observation can lead to the controlling and tuning the photoluminescence, which is highly desirable for optoelectronics and gas sensing applications.

School of Physics  
Academic Year 2022

Student's Signature   
Advisor's Signature   
Co-Advisor's Signature 

## ACKNOWLEDGEMENTS

This thesis was completed with the help and support of several people. First and foremost, I would like to express my sincere gratitude to my advisor, Assoc. Prof. Dr. Worawat Meevasana who guided, instructed, and motivated me. He provided this opportunity and led me along the path of research under his supervision. He is an excellent advisor due to his kindness, dedication, and encouragement. I learned a great deal from him, including the research process, research planning, data analysis, and time management. He has helped and supported me through every step to get to where I am today. Also, I would like to express my deepest gratitude to my co-advisor, Dr. Sorawis Sangtawesin, who was always beside me and believed in my potential to pass through all the difficulties in this thesis. Without their encouragement and motivation from him, I would not have been able to complete this journey. Their expertise and patience have been invaluable to me and have played a crucial role in the success of this thesis. He shares knowledge and good scientific skills with me, including attitudes towards various aspects such as time management. Apart from being an excellent advisor, he is also an idol in my life.

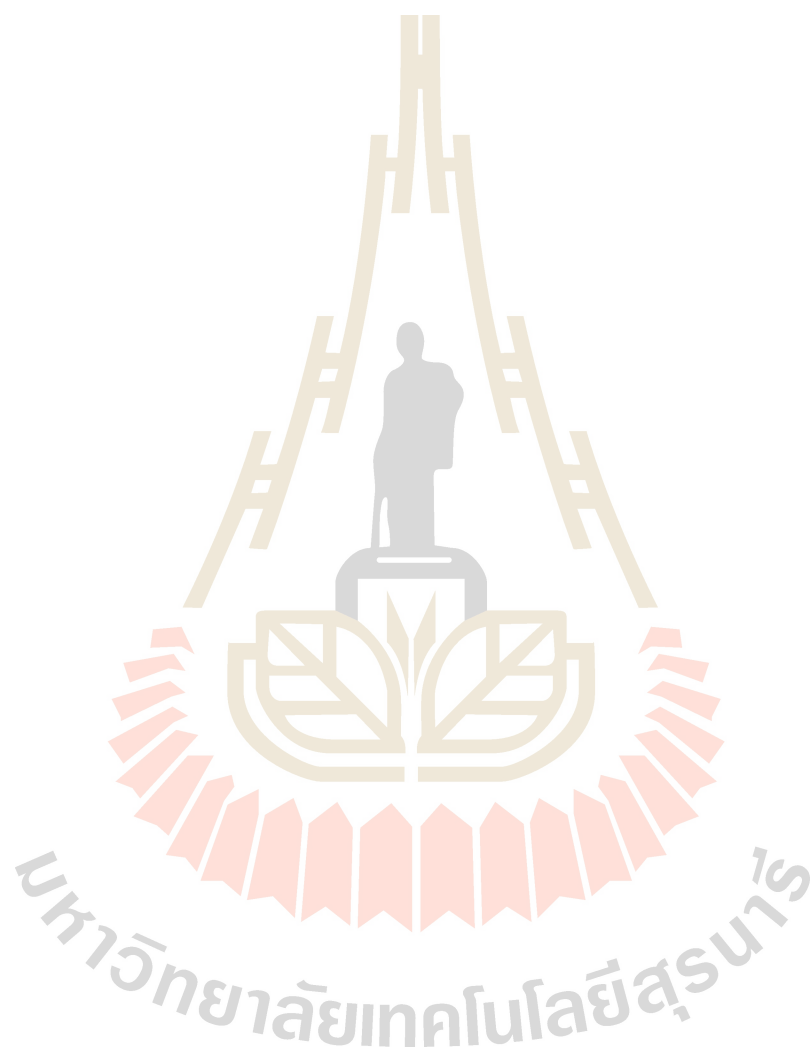
For my defense, I would like to acknowledge Assoc. Prof. Dr. Panomsak Meemon, Assoc. Prof. Dr. Prayoon Songsiritthigul, and Asst. Prof. Dr. Sukrit Sucharitakul for giving their valuable time, reviewing my thesis, and providing constructive feedback during my Ph.D. defense.

Importantly, I would like to acknowledge the Science Achievement Scholarship of Thailand (SAST) for providing financial support while pursuing my bachelor's degree and this research has received funding support from the NSRF via the Program Management Unit for Human Resources & Institutional Development, Research and Innovation [B05F640051, B05F650024].

Also, I would like to thank everyone in the Meevasana Group, QLAB, OCT lab, Synchrotron Light Research Institute (SLRI), Facility Building 10 (F10), all the staff and students in the School of Physics (SUT) for always being beside and support me.

Last but not least, I am indebted to my parents and brother for unwavering support, understanding, and motivation during this challenging journey. Their belief in my abilities has been a driving force that propelled me forward.

Aissara Rasritat





# CONTENTS

	Page
ABSTRACT IN THAI .....	I
ABSTRACT IN ENGLISH .....	II
ACKNOWLEDGEMENTS.....	III
CONTENTS .....	V
LIST OF FIGURES .....	VII
<b>CHAPTER</b>	
<b>I INTRODUCTION.....</b>	<b>1</b>
1.1 Background and motivation.....	1
1.2 Research objectives.....	2
1.3 Outline of thesis.....	3
<b>II LITERATURE REVIEWS .....</b>	<b>4</b>
2.1 Transition metal dichalcogenides .....	4
2.1.1 Molybdenum disulfide.....	7
2.2 The electronic band structure and the photoluminescence of TMDs.....	8
2.2.1 The electronic band structure.....	8
2.2.2 The photoluminescence.....	9
2.2.3 Quenching of fluorescence.....	11
2.2.4 Exciton .....	12
2.2.5 Trion.....	13
2.3 Defects in TMDs.....	15
2.4 Electron irradiation .....	19
2.5 Vibrational properties of TMDs .....	21
<b>III MATERIALS AND METHODOLOGY.....</b>	<b>23</b>
3.1 Electron beam irradiation preparation.....	23
3.2 Confocal microscopy.....	24
3.3 Raman spectroscopy.....	26

## CONTENTS (Continued)

	Page
3.4 The photoluminescence spectroscopy under N <sub>2</sub> .....	27
3.5 Processed photoluminescence data .....	29
<b>IV RESULTS AND DISCUSSION.....</b>	<b>31</b>
4.1 Photoluminescence spectroscopy observation.....	31
4.2 Raman spectroscopy observation.....	40
4.3 Analysis of photoluminescence spectra.....	44
<b>V CONCLUSION AND FUTURE RESEARCH.....</b>	<b>51</b>
5.1 Conclusions .....	51
5.2 Improvement and future research.....	52
REFERENCES .....	53
APPENDIX.....	59
CURRICULUM VITAE.....	64

## LIST OF FIGURES

Figure	Page
2.1 Atomic structure of single layer of transition metal dichalcogenides .....	6
2.2 Top-view and side-view of atomic structure of MoS <sub>2</sub> .....	7
2.3 The calculation band structures of MoS <sub>2</sub> .....	8
2.4 PL spectra for mono- and bilayer MoS <sub>2</sub> samples.....	9
2.5 Raman and photoluminescence spectra of MoS <sub>2</sub> monolayer, bilayer, hexalayer, and bulks.....	11
2.6 PL spectrum of MoS <sub>2</sub> at 273 K .....	15
2.7 PL spectra of monolayer MoS <sub>2</sub> after oxygen plasma irradiation with different durations.....	17
2.8 Time-dependent photoluminescence (PL) spectra of plasma-treated monolayer MoS <sub>2</sub> .....	18
2.9 Raman peak shift vs S vacancy.....	20
2.10 Schematic illustration of in-plane phonon modes E' and the out-of-plane phonon mode A <sub>1g</sub> , for the bulk MoS <sub>2</sub> .....	21
2.11 Thickness-dependent Raman spectra for MoS <sub>2</sub> .....	22
3.1 Schematics of electron beam irradiation on monolayer MoS <sub>2</sub> by SEM at ultralow energy with 5 kV accelerating voltage.....	23
3.2 Diagram of confocal microscope setup .....	25
3.3 SENTERRA II Dispersive Raman microscope from Bruker Optics.....	27
3.4 Diagram of a confocal microscope setup under N <sub>2</sub> .....	28
3.5 The experiment setup.....	28
3.6 The unprocessed photoluminescence data of monolayer MoS <sub>2</sub> .....	29
3.7 The normalized data after subtracting data .....	30
4.1 The spectrum of pristine monolayer MoS <sub>2</sub> .....	32
4.2 The confocal PL intensity image of pristine monolayer MoS <sub>2</sub> .....	32



## LIST OF FIGURES (Continued)

Figure	Page
4.3 Confocal PL intensity image of the irradiated sample showing e-beam irradiated regions by SEM at 5 kV accelerating voltage.....	33
4.4 Comparison of the PL spectrum of pristine, electron irradiated dose of $0.3 \times 10^3 \mu\text{C}/\text{cm}^2$ and $5.3 \times 10^3 \mu\text{C}/\text{cm}^2$ .....	34
4.5 Schematics of laser exposure on monolayer MoS <sub>2</sub> under ambient. ....	35
4.6 Confocal PL intensity image of pristine, low electron dose and high electron dose of monolayer MoS <sub>2</sub> before and after high power exposure for 10 s when storing in the ambient air for 10 hours. ....	36
4.7 The relative PL intensity with varying different condition after high power exposure and storing in ambient air for 10 hours .....	37
4.8 The PL spectra of the electron irradiation area after exposure.....	39
4.9 The PL intensity under N <sub>2</sub> and ambient air.....	40
4.10 The Raman spectrum of pristine of monolayer MoS <sub>2</sub> .....	41
4.11 Raman spectra of different conditions.....	42
4.12 Raman peak positions of E <sub>2</sub> and A <sub>1</sub> modes.....	43
4.13 The PL spectrum before and after exposure .....	44
4.14 The PL spectrum under N <sub>2</sub> for at 15 minutes and 10 hours .....	45
4.15 The PL spectrum at 25 minutes under ambient air.....	46
4.16 The PL spectrum at 10 hours under ambient air .....	47
4.17 The relative peak area as a function of time under N <sub>2</sub> and ambient conditions .....	48
4.18 The schematic and confocal models show that oxygen molecules absorb on the surface. ....	50
A.1 Confocal images of monolayer MoS <sub>2</sub> with electron irradiation doses variation .....	60
A.2 The relative PL intensity of the areas exposed by different electron irradiation dose .....	61
A.3 Relative PL intensity of electron dose irradiation $D = 0.2 \times 10^3 \mu\text{C}/\text{cm}^2$ .....	62

## LIST OF FIGURES (Continued)

Figure	Page
A.4 Relative PL intensity of electron dose irradiation $D = 2.0 \times 10^3 \mu\text{C}/\text{cm}^2$ .....	63



# CHAPTER I

## INTRODUCTION

### 1.1 Background and motivation

Semiconducting transition metal dichalcogenides (TMDs) materials with high carrier mobility, high ON/OFF current ratio, and versatility have been attractively studied to replace the silicon-based semiconductors (Bhimanapati et al., 2015; Mattheiss et al., 1973). They exhibit unique physical and optical properties such as the transition from indirect to direct bandgap upon thinning down from bulk to monolayer, which are essential for designing the electronic and optoelectronic devices (Mak et al., 2010). For example, the ultrathin MoS<sub>2</sub> layer exhibits intense photoluminescence and tunable bandgap. These behaviors are applicable in tunable optical platforms including phototransistors (Lee et al., 2012; Yin et al., 2011), photodetectors (Lopez-Sanchez et al., 2013), and gas sensors (Kumar et al., 2020).

Furthermore, Raman spectroscopy may be used as a quantitative diagnostic tool to characterize MoS<sub>2</sub>-based transport channels (Splendiani et al., 2010). The replacement of the main metal oxide by 2D materials has also been demonstrated by their efficacy in gas sensing, with detection down to 1 ppb concentration of distinct gases (NO<sub>2</sub>, NH<sub>3</sub>, CO, and H<sub>2</sub>O) and detection to even single gas molecule in ambient condition. For example, Schedin et al. utilized graphene, established the first gas sensor (Schedin et al., 2007). Among the all 2D materials, MoS<sub>2</sub> stands out as one of the most promising layered materials for the development of gas sensors due to its remarkable attributes, such as a high surface-to-volume ratio, substantial adsorption coefficient, and distinctive thickness-dependent electrical and chemical properties. Li et al. studied the gas and MoS<sub>2</sub> interaction by fabricating FET sensors from the monolayer, 2 layers, 3 layers, and 4 layers of the MoS<sub>2</sub> (Li et al., 2012).

Another work, Late et al. studied the FET gas sensor from a monolayer to a multilayer MoS<sub>2</sub> using the mechanical exfoliation technique and found that monolayer of MoS<sub>2</sub> exhibited an unstable current response over time.



The NO and NH<sub>3</sub> sensing responses of 3, 4, and 5 layers MoS<sub>2</sub> at room temperature were compared and they found that the 5 layers MoS<sub>2</sub> showed higher sensitivity to gas than 2 layers MoS<sub>2</sub>. They explained the result by analyzing the resistance of n-type MoS<sub>2</sub>, which changes after adsorption of NO<sub>2</sub> or NH<sub>3</sub> due to the charge transfer mechanism. NO<sub>2</sub> in nature, which contains an unpaired electron on the N atom, removes electrons from MoS<sub>2</sub>, which then shifts the Fermi level closer to the valence band. MoS<sub>2</sub> is more sensitive to NO<sub>2</sub> than NH<sub>3</sub> because the adsorption energy of NO<sub>2</sub> is greater than that of NH<sub>3</sub> (Late et al., 2013).

Further studies of the charge transfer mechanism, conducted by Cho et al. via in-situ photoluminescence (PL) experiments, show that the electronic interaction between NO<sub>2</sub> and MoS<sub>2</sub> converts the neutral (A and B) excitons into a quasi-particle trion by creating a hole through the extraction of another electron. Conversely, NH<sub>3</sub> interaction dissociated the trion into neutral excitons by providing electrons to MoS<sub>2</sub>. Consequently, in the PL spectra, the trion peak intensity increased (decreased) upon NO<sub>2</sub> (NH<sub>3</sub>) interaction with MoS<sub>2</sub>, while the opposite occurred for the neutral exciton peak intensity (Cho et al., 2015).

Many researchers have put efforts into studying and have found exciting sensing results from MoS<sub>2</sub> gas sensors, however there is still a need to optimize the surface, atomic structure, and electronic structure for better sensitivity. A comprehensive understanding of the gas sensing mechanism requires a more detailed analysis, including a multitude of variables including surface states, edge locations, defects, crystallinity, strain, electrical, and chemical properties. Therefore, in this work, we would like to study the bandgap engineering of the monolayer MoS<sub>2</sub> surface via photoluminescence methods. We modify the surface by electron irradiation, using low energy SEM, and use confocal microscopy to study the photoluminescence of the resulting surface.

## 1.2 Research objectives

- 1.2.1 To study the variation of photoluminescence of monolayer TMDs after electron irradiation via SEM.

- 1.2.2 To study the variation of photoluminescence of monolayer TMDs that was electron irradiated after high power laser exposure.
- 1.2.3 To understand the mechanism that the photoluminescence intensity of MoS<sub>2</sub> decreases after high-power laser exposure and can recover when stored to ambient air.

### 1.3 Outline of thesis

This thesis is divided into five main chapters. Chapter I is the introduction that includes the background, motivation, and research objectives. In chapter II, we describe the fundamental structure, the electronic band structure, the photoluminescence of TMDs, defect in TMDs, and the effect of electron irradiation on the TMD surfaces. In chapter III, we describe the preparation of samples irradiated with electron via low energy SEM. Moreover, we explain the basics of confocal microscopy and Raman spectroscopy. Chapter IV presents the experimental results consisting of basic, monolayer characterizations, the behavior after electron irradiation and photoluminescence after high power laser exposure onto the sample. Moreover, we discuss the recovery of photoluminescence intensity after high power laser exposure and storage in the ambient condition. Finally, the conclusions of this thesis are given in Chapter V.

## CHAPTER II

### LITERATURE REVIEWS

This chapter describes the properties of transition metal dichalcogenides (TMDs) including the structure, photoluminescence properties, band structure engineering. The effect of electron irradiation and laser exposure on the surface is also described.

#### 2.1 Transition metal dichalcogenides

Two-dimensional transition metal dichalcogenides (TMDs) are an emerging class of materials with highly desirable properties for investigating novel physical phenomena and exploring various applications, including nanoelectronics, nanophotonics, and sensing. In recent years, there have been notable resurgence of interest in TMDs, because of the demonstration of the first transistor and the subsequent discovery of strong photoluminescence in monolayers of MoS<sub>2</sub> (Radisavljevic et al., 2011). In 1923, Pauling et al. created the first discovery of their unique structure, which contains MoS<sub>2</sub> in the form of a hexagonal unit (Pauling et al., 1923). In 1963, Frindt et al. studied the use of adhesive tapes exfoliation to create ultrathin MoS<sub>2</sub> layers (Frindt et al., 1963), and in 1986, the first monolayer MoS<sub>2</sub> suspensions were produced (Joensen et al., 1986). In general, TMDs have different shapes because the transition metal atoms are in different coordination spheres, as shown in Figure 2.1. These structural phases can also be described in terms of the specific layered structures with three atomic planes (chalcogen, metal, and chalcogen) that compose the individual layers of these materials. TMDs can exist in several phases, depending on the combination of transition metal and chalcogen elements. The 2H phases are characterized by an ABA stacking structure.

--Chalcogen atoms (A) from distinct atomic planes occupying the same position are vertically aligned with each other across the direction perpendicular to the layer, and transition metal atoms (B) are sandwiched in between the chalcogen layers. On the other hand, 1T phases exhibit an ABC stacking pattern, and the other phase 1T' can often be obtained as a metastable phase.

The thermodynamic stability of the phase in TMD compounds is dependent on the specific combination of transition metal elements from groups IV, V, VI, VII, IX, or X, along with the chalcogen elements sulfur (S), selenium (Se), or tellurium (Te). From the possibility of chemically different bulk TMDs produced by group VI elements, specifically molybdenum (Mo) or tungsten (W), it has been observed that the 2H phase is thermodynamically stable for five out of the six possible combinations. In the case of multilayer and bulk samples, the structure of TMDs is further defined by the layering configuration of the individual layers, and by possible distortions that lower periodicity. These distortions can form the metal-metal bond. For example, the dimerization of the 1T phase of group VI TMDs can lead to the formation of the 1T' phase. Similarly, the tetramerization of rhenium dichalcogenides, such as 1T-ReS<sub>2</sub>, can also form the 1T' phase (Geim et al., 2013). These imperfections are still challenges that need to be addressed, to improve the TMDs stability and scalability for industrial applications.

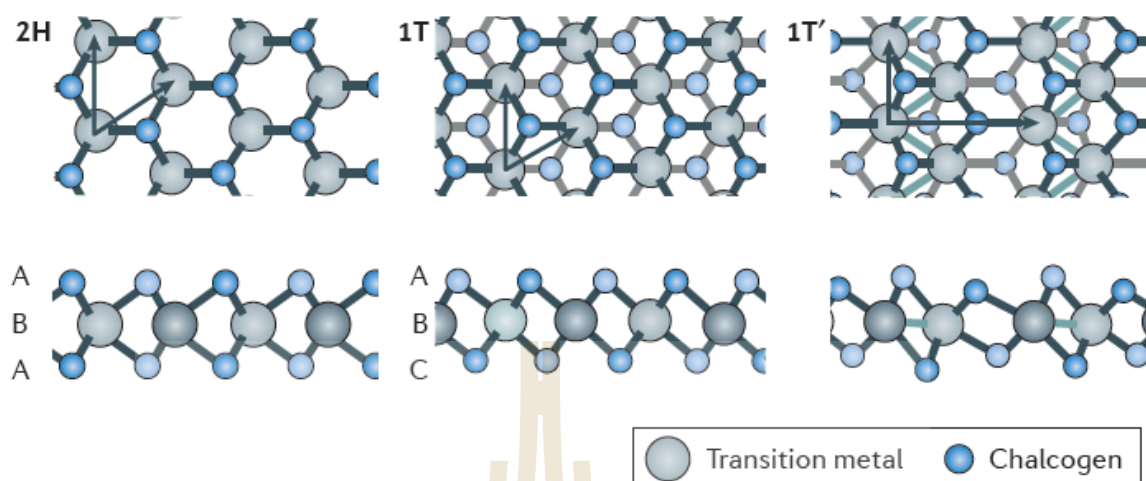


**Figure 2.1** Atomic structure of monolayer of transition metal dichalcogenides (TMDs) in their trigonal (2H), octahedral (1T) and dimerized (1T') phases (Geim et al., 2013).

The layer-dependent characteristics of TMDs have gathered significant attention in recent research. In various TMDs, when a material is changed from a bulk to a monolayer, a shift from an indirect bandgap to a direct bandgap can be seen. For example, in the case of  $\text{MoS}_2$ , the bulk form of the material has an indirect bandgap of 1.3 eV, while the monolayer form has an increased direct bandgap of 1.8 eV (Ganatra et al., 2014). Atomically thin and processable, these materials are of significant interest in many kinds of optoelectronics applications. Flexible and transparent optoelectronics exhibit significant potential. Optoelectronics devices encompass a range of electronic devices that include the ability to generate, detect, interact with, or regulate light. Typical examples of such devices include lasers, light-emitting diodes (LEDs), solar cells, optical switches, photodetectors, and displays. Extensive research has been conducted on the different possible uses of TMDs in the sectors of photovoltaics and photodetectors. The photosensitivity of  $\text{MoS}_2$  and  $\text{WS}_2$  thin films demonstrates their potential for light-sensitive applications. Yin et al. studied  $\text{MoS}_2$  layers of different thickness that can absorb light at different wavelengths. The photocurrent of this device exhibits a dependence on the intensity of incident light and exhibits an instantaneous response of 50 ms to changes in light levels, while also exhibiting a notable level of photoresponsivity. The results pave the way for developing monolayer semiconducting materials for optoelectronics device applications in the future (Yin et al., 2012).



### 2.1.1 Molybdenum disulfide

Molybdenum disulfide ( $\text{MoS}_2$ ), an inorganic compound within the TMDs category, has gathered significant attention.  $\text{MoS}_2$  consists of one atom of Molybdenum (Mo) and two atoms of Sulfur (S).  $\text{MoS}_2$  has a layered structure with molybdenum atoms sandwiched between two layers of sulfur atoms. The structure of  $\text{MoS}_2$  crystals consists of layers that are vertically stacked and held together by van der Waals forces, which are relatively weak interactions between molecules. Its 2H phase is thermodynamically stable and aligns with an ABA stacking structure (Radisavljevic et al., 2011).

Atomic structures of  $\text{MoS}_2$  are shown in Figure 2.2. As the thickness decreases, the position of the valence band and conduction band edges are shifted, transitioning from an indirect bandgap in its bulk form to a direct bandgap in its monolayer form. (Splendiani et al., 2010). This property drew attention to these material for gate-tunable electronic devices (Radisavljevic et al., 2011). Remarkably, the monolayer 2H-  $\text{MoS}_2$  lacks inversion symmetry, instigating a spin splitting phenomenon in the electronic band structure, driven by the intricate interplay of spin-orbit interactions. Notably, the absence of time reversal invariant momenta at points K and K' breaks the spin degeneracy at the conduction and valence band, with the valence band experiencing a pronounced spin splitting effect (Zhu et al., 2011). This intrinsic property of TMDs may be used to design spintronic devices (Pulkin et al., 2016).

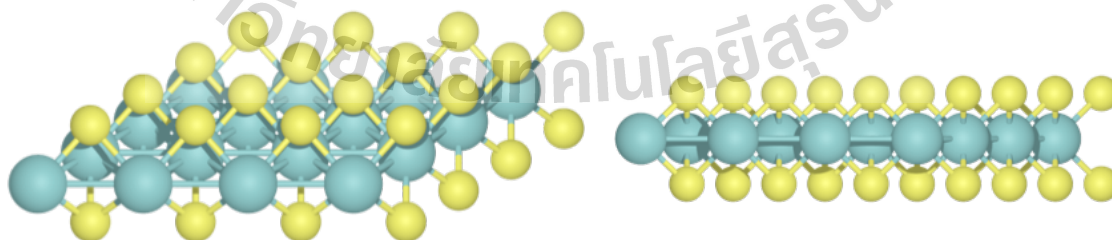


**Figure 2.2** a) Top view of atomic structure of  $\text{MoS}_2$  where green spheres represent a transition metal (Mo) and yellow spheres represents a chalcogen (S). b) Side view of atomic structure of  $\text{MoS}_2$ .

Moreover, MoS<sub>2</sub> has been attractively studied as one of the prominent layered TMDs. The properties of individual layers of MoS<sub>2</sub> differ significantly from its bulk form. When interlayer interactions are eliminated, and electrons are confined to a mono plane. Interestingly, a monolayer of MoS<sub>2</sub> can absorb up to 10% of incident light with energy higher than the bandgap, and a dramatic increase in photoluminescence intensity is observed when compared to a bulk crystal (Piper et al., 2016). This unique property of MoS<sub>2</sub> is quite inspiring as it effectively addresses the limitations of gapless graphene and opens possibilities for the utilization of 2D materials in the development of advanced switching and optoelectronics devices for the next generation.

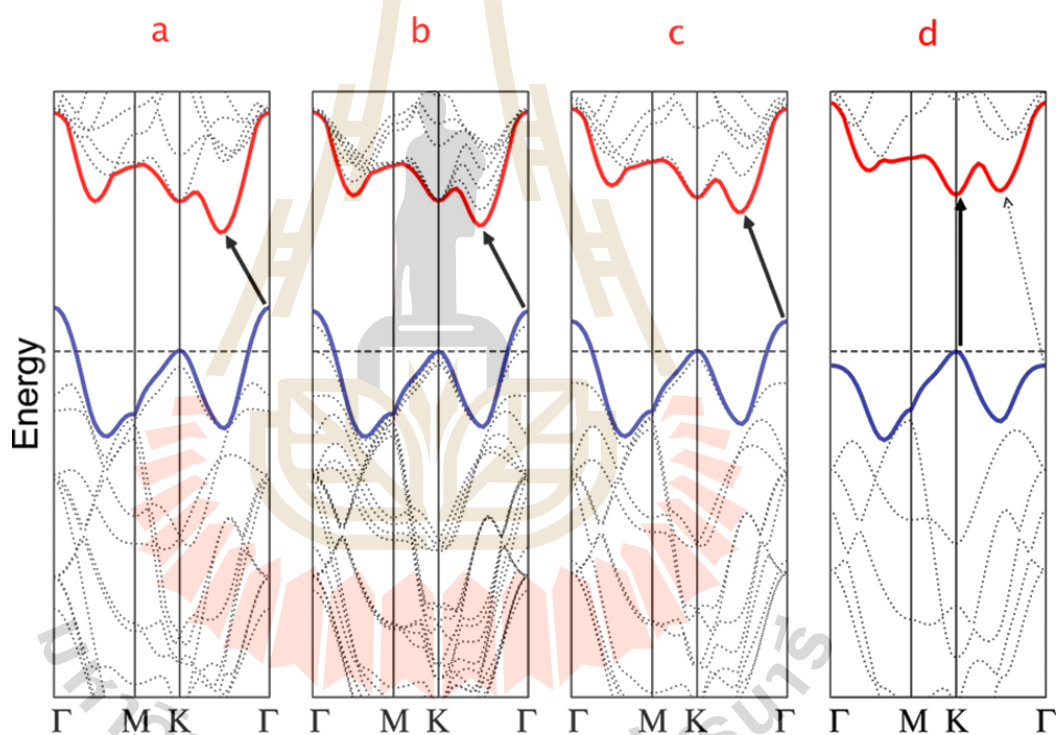


**Figure 2.3** The calculated band structures of bulk MoS<sub>2</sub>, quadrilayer MoS<sub>2</sub>, bilayer MoS<sub>2</sub>, and monolayer MoS<sub>2</sub> from left to right (Ellis et al., 2011).

## 2.2 The electronic band structure and the photoluminescence of transition metal dichalcogenides

### 2.2.1 The electronic band structure

In general, bulk TMDs consist of stacked monolayers MX<sub>2</sub> where M is a metal transition atom and X is a chalcogen atom that are bonded through weak van der Waals forces in the out-of-plane direction. Within each monolayer, there are three

stacked layers (X-M-X) of atoms held together by strong covalent bonds. In the case of MoS<sub>2</sub>, the bulk form has an indirect band gap at 1.2 eV. As the number of layers decreases, strong confinement in the out-of-plane direction results in the transition from an indirect to a direct band gap at 1.8 eV, as shown in Figure 2.3. The varying of the number of layers in MoS<sub>2</sub>, from multilayer to monolayer, show a qualitative alteration of the band structure, which in turn provides a explanation for the pronounced photoluminescence (PL) effect observed in monolayer samples (Ellis et al., 2011).

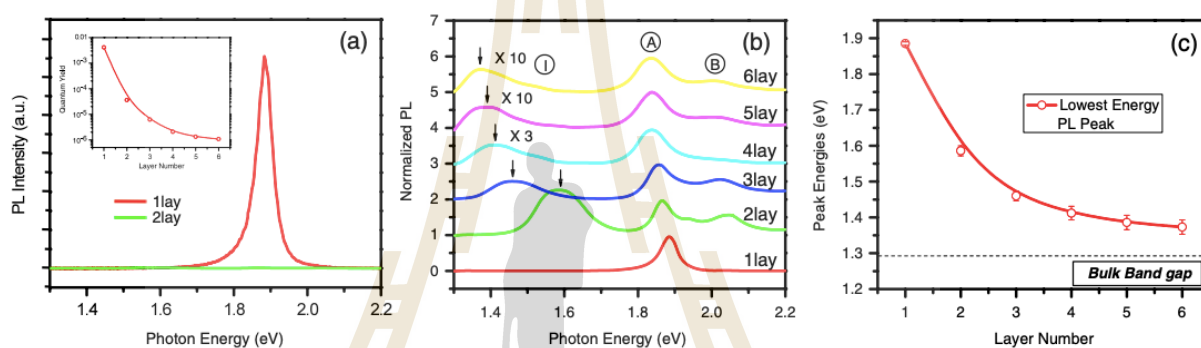


**Figure 2.4** (a) Photoluminescence spectra for mono- and bilayer of MoS<sub>2</sub>. Inset: photoluminescence quantum yield of thin layers for 1–6. (b) Normalized PL spectra by the intensity of peak A of thin layers of MoS<sub>2</sub>. (c) Band gap energy of MoS<sub>2</sub> when increase thickness. The dashed line represents the (indirect) band gap energy of bulk MoS<sub>2</sub> (Mak et al., 2011).

## 2.2.2 The photoluminescence

Photoluminescence (PL) is an interesting effect because photoluminescence can explain the relationship between electronic properties and optical properties. The PL technique involves detecting the light that emits from the material. In this technique, we shine the light on the sample, electrons absorb the light and are excited the conduction band, then relax back to the valence band and emit photon.

Mak et al. studied that the electronic attributes of ultrathin molybdenum disulfide crystals, encompassing 1 – 6 S-Mo-S monolayers, employing optical spectroscopy as the tool of analysis. This study investigates the effect of quantum

confinement on the electronic structure of the material through the utilization of absorption, photoluminescence, and photoconductivity spectroscopy. As the thickness decreases, the indirect band gap, which is located below the direct gap in the bulk material, undergoes an upward energy shift of nearly 0.6 eV. This remarkable transformation leads to a transition to a direct-gap configuration in the monolayer, depicted in Figure 2.4. Consequently, the quantum yield increase was observed, approaching  $10^4$  fold in monolayer  $\text{MoS}_2$ . The PL spectra observed exhibit a dependence on the layer number. However, the band gap demonstrates a decreasing trend as the number of layers increases (Mak et al., 2011).

Moreover, Splendiani et al. have reported the distinct PL difference between monolayer, bilayer, quadrilayer and hexalayer samples in Figure 2.5. The transition of  $\text{MoS}_2$  from bulk to a monolayer is characterized by the formation of known resonances in the monolayer sample. These resonances are indicative of direct excitonic transitions occurring in near proximity to the Brillouin zone K point. Specifically, the spectra for monolayer  $\text{MoS}_2$  shows two distinct PL peaks at 670 nm and 627 nm, which are known as A and B excitons. The separation of two excitons are associated with the spin-orbital coupling of the valence band. This observation aligns with the theoretical prediction of a bandgap transition from an indirect band gap with an energy of 1.2 eV to a direct band gap with an energy of 1.8 eV (Splendiani et al., 2009).

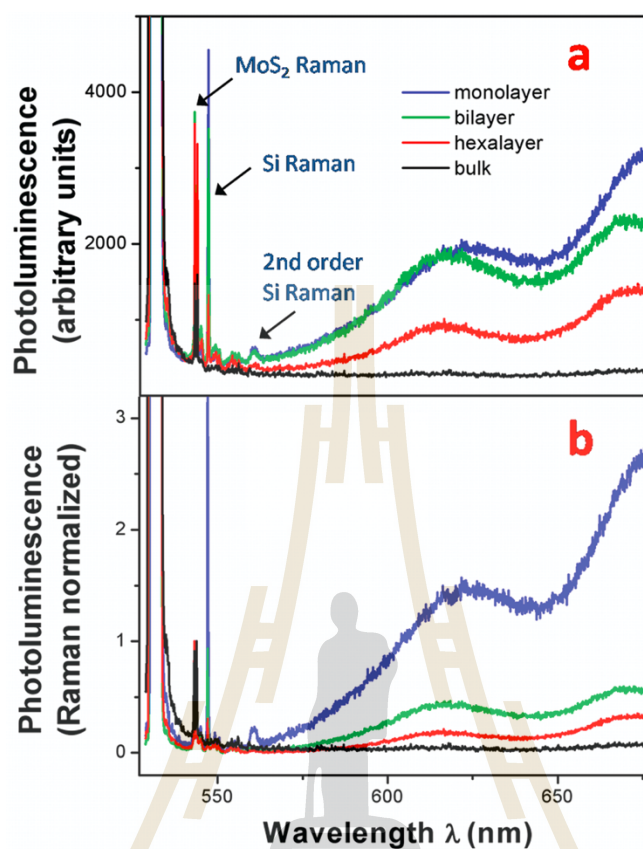


**Figure 2.5** (a) Photoluminescence spectra of bulk, hexalayer, bilayer, and monolayer of MoS<sub>2</sub>. Raman peaks can be attributed to distinct vibrational modes of MoS<sub>2</sub>. For thin MoS<sub>2</sub> layers, the monolayer MoS<sub>2</sub> Raman spectrum is relatively weak because less material is excited. Despite the reduced material, the photoluminescence is highest in monolayer MoS<sub>2</sub>. (b) The photoluminescence spectra of MoS<sub>2</sub> layers, normalized by the Raman intensity. It was found that the luminescence efficiency of monolayer MoS<sub>2</sub> exhibited a significant increase (Splendiani et al., 2009).

### 2.2.3 Quenching of fluorescence

Quenching refers to any process that suppresses the fluorescence intensity of a sample. In quenching, many kinds of molecular interactions may occur through various mechanisms, including energy transfer, excited-state reactions, molecular rearrangements, the formation of ground state structures, and collisional quenching.

Several different kinds of substances act as fluorescence quenchers. Among the most known collisional quenchers is molecular oxygen, which quenches almost all known fluorophores (Kautsky 1939). Kang studied that oxygen plasma treatment



leads to the creation of defect in monolayer MoS<sub>2</sub>, resulting in the quenching of photoluminescence intensity (Kang et al., 2014).

Bhanu studied that the interaction between pristine MoS<sub>2</sub> and Au nanoislands, resulting in local variations of photoluminescence (PL) in Au-MoS<sub>2</sub> hybrid structures. The PL spectra of pristine MoS<sub>2</sub> showed variations in peak intensity and position, but no quenching was observed. After depositing of Au (2.0 nm) on MoS<sub>2</sub>, the PL quenching was observed throughout the flake, indicating a strong charge transfer interaction between Au and MoS<sub>2</sub>. This PL quenching was attributed to the p-doping of MoS<sub>2</sub> caused by charge transfer from MoS<sub>2</sub> to Au, and the results suggest the potential for new avenues in 2D nanoelectronics and active control of transport or catalytic properties (Bhanuu et al., 2014).

In addition to that, the photoluminescence (PL) intensity of monolayer MoS<sub>2</sub> can be quenched by the adsorption of n-type dopants such as nicotinamide adenine dinucleotide (NADH) molecules, resulting in a decrease in the exciton PL intensity and an increase in the trion PL intensity. (See section 2.2.4 and 2.2.5 for details.) The quenching of PL in monolayer MoS<sub>2</sub> can also be induced by FET gate doping, similar to the behavior observed with chemical doping. The suppression of PL intensity in monolayer MoS<sub>2</sub> by n-type dopants suggests that the electrons from the dopant are additionally doped into the material (Mouri et al., 2013).

#### 2.2.4 Exciton

An exciton is a bound state of a positively charged hole and a negatively charged electron, attracted to each other by the electrostatic Coulomb force (Elliott et al., 1957). This electrically neutral quasiparticle is mostly found in semiconductors and is created through photoexcitation. Excitons play a key role in light emission and recombination due to their strong interaction with light. (Cirtin et al., 1993). In low-dimensional crystals, weak dielectric screening and strong geometrical confinement enhance the Coulomb interaction, leading to various many-particle phenomena such as bright excitons, dark excitons, and trions. The nature of excitons, whether bright or dark, depends on the spin orientation of the electron and hole. If the electron and hole have opposite spins, they can easily recombine and emit a photon, forming a

bright exciton. If they have the same spin, they cannot easily recombine due to the lack of spin momentum conservation, resulting in dark excitons. Dark excitons, which do not emit light and thus cannot relax to a lower energy level, are promising qubits (Xiaoyang et al., 2019).

For the  $\text{MoS}_2$ , from the transition, these two resonances have been well established. The energy differential between the two resonances is a result of the valence band spin-orbital separation, known as A and B excitons (Coehoorn et al., 1987). The transition probabilities of the A exciton are higher than those of the B exciton due to its resonance with lower energy (Mak et al., 2010). Consequently, the PL spectrum are the presence of two prominent resonances, known as A and B excitons, which are related to the spin degeneracy of the valence band. The splitting in the conduction band is relatively small, but in the valence band, the separation is about 200 meV (Kormanyos et al., 2015).

### 2.2.5 Trion

Trion are 3 quasiparticle that can capture an additional charge to form charge exciton. It can be capture negative or positive depending on its charge state: a negative trion (negative e-e-h) is a complex of two electron and one hole and a positive trion (negative e-h-h) is a complex of two holes and one electron. In addition, Mak et al. studies that a monolayer  $\text{MoS}_2$  field-effect transistor. The spectroscopic identification of a tightly bound negative trion. These unique quasiparticles, which can be optically created with valley and spin polarized holes, do not have any counterpart in conventional semiconductors. They exhibit a binding energy of approximately 20 meV, making them highly relevant even at room temperature (Mak et al., 2012). Lui et al. studied that to differentiate between the trion and electron contributions to the photoconductivity, giving direct evidence of trion transport. These preliminary observations show that trion has pseudospin and charge and is abundant. When  $\text{MoS}_2$  is excited by light. Due to being vulnerable to control by electric fields and polarization, trion transport, density, and pseudo-spin exhibit attractive features for potential

utilization in scientific and technological applications (Lui et al., 2014). Moreover, Christopher et al. studied monolayer  $\text{MoS}_2$  has emerged as a system for investigating many-body physics due to its reduced dimensionality, which leads to tightly bound states stable at room temperature, as screening effects are reduced. The pseudo-spin degree of freedom is exhibited by the many-body states and relates to the two direct-gap valleys found in the band structure. This characteristic presents possibilities for optical manipulation. By analyzing this spectral using a Lorentzian peak, the component corresponding to the spectra of A exciton, B exciton, and trion at the end of a long tail was found are shown in Figure 2.6. As indicated in the component, the emergence of A and B excitons can be attributed to the spin-orbit splitting of the valence band. On the other hand, a trion is created when an exciton interacts with either an electron or a hole. They focus on negatively charged trion, which are stable even at room temperature due to the high unintentional doping of  $\text{MoS}_2$ . The trion at low-energy tail length depends on two factors: the trion thermal momentum distribution, and the bound state wave function. Trion can radiatively decay with non-zero momentum by ejecting an electron. The results show that an asymmetric photoluminescence (PL) peak with a long low-energy tail and a peak position that shifts from the zero momentum trion energy. Understanding the asymmetry of the trion PL peak and its subsequent peak red shift is essential. It depends on both the trion size and a temperature dependent contribution. Neglecting this asymmetry could lead to an overestimation of the trion binding energy by nearly 20 meV at room temperature. To shed light on these phenomena, they perform a detailed analysis of the temperature dependent PL, which reveals the effective trion size, consistent with existing literature, and provides insights into the temperature dependence of the band gap and spin-orbit splitting of the valence band. Importantly, this study represents the first comprehensive analysis of the temperature-dependence of trion PL with such precision, offering valuable insights into the behavior of this intriguing system

(Christopher et al., 2017).

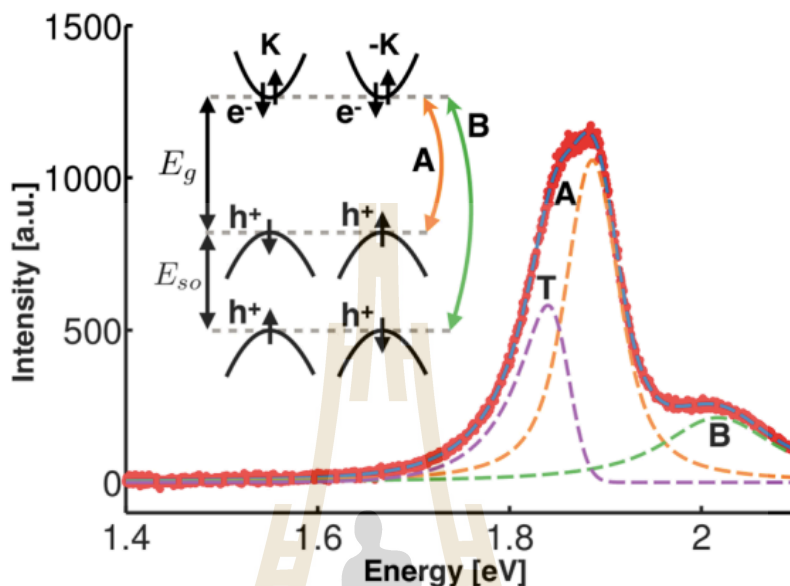


**Figure 2.6** PL spectrum of MoS<sub>2</sub> at 273 K (background subtracted). A and B denote excitons, and T denotes the trion (Christopher et al., 2017).

### 2.3 Defects in TMDs

Sefaattin et al. studied that point of defect in semiconductor can trap free charge carriers and localizes excitons. The interaction between these defects and charge carriers becomes stronger at reduced dimension and modify the optical properties of monolayer TMDs. This includes an enhancement of the overall integrated PL intensity and the appearance of a new, defect-related peak below the band gap. The observed enhancement in photoluminescence (PL) intensity can be attributed to the electrical influence of defects in the material. These defects allow the transfer of free electrons from the material to gas molecules, leading to a transition in the population of excitons from charged to neutral states, including both free and bound excitons (Sefaattin et al., 2013). Another work, Nan et al. studied that oxygen irradiated on MoS<sub>2</sub> samples created S vacancy. That causes the PL intensity to increase with exposure duration, as shown in Figure 2.7. The binding energy between an O<sub>2</sub> molecule

and  $\text{MoS}_2$  is 0.102 eV, indicating a state of physical adsorption. Conversely, when an  $\text{O}_2$  molecule binds to a sulfur (S) vacancy on  $\text{MoS}_2$ , the binding energy significantly increases to 2.395 eV. The calculations to determine the energy barrier between physical and chemical adsorption of oxygen molecules on the  $\text{MoS}_2$  vacancy. The results revealed a reaction barrier of approximately 1.05 eV. While this barrier poses a challenge under normal conditions, it can be easily increased through high-temperature annealing, the transition from physical to chemical adsorption of oxygen molecules on the  $\text{MoS}_2$  vacancy. The photoluminescence (PL) is enhanced due to the process of oxygen chemical adsorption, which leads to strong p-doping. This process also facilitates the conversion of trion to excitons and reduces nonradiative recombination of excitons at defect sites. The verification of these phenomena was conducted using low-temperature PL measurements. First principle demonstrates a significant binding energy of 2.395 eV for the adsorption of an oxygen molecule onto a sulfur vacancy site on a  $\text{MoS}_2$  surface. The oxygen molecules that are adsorbed chemically also exhibits a significantly higher efficiency in terms of charge transfer (0.997 electrons per  $\text{O}_2$ ) when compared to physically adsorbed oxygen molecules on an  $\text{MoS}_2$  surface. The achievement of defect engineering and oxygen bonding can be simply accomplished with the use of oxygen plasma irradiation. The development of Mo-O bonding has been verified via X-ray photoelectron spectroscopy (Nan et al., 2014).



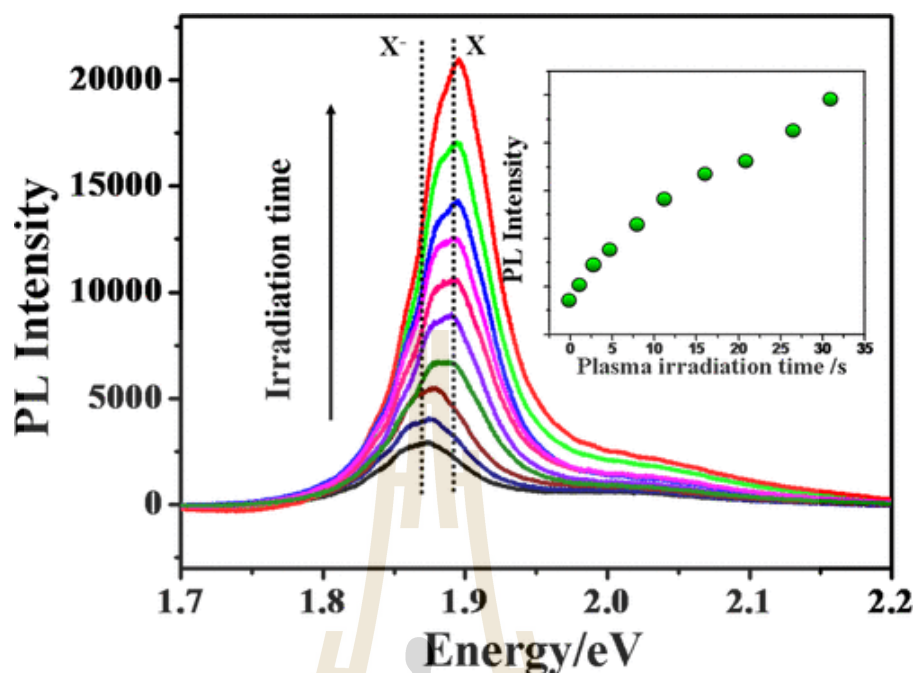


**Figure 2.7** The photoluminescence spectra of monolayer  $\text{MoS}_2$  were measured after exposure to oxygen plasma for different durations. The variation of photoluminescence (PL) intensity with plasma irradiation times can be seen in the inset (Nan et al., 2014).

Moreover, the detailed structural investigation demonstrates that inside the  $\text{MoS}_2$  compound, one oxygen molecule ( $\text{O}_2$ ) is located at the S vacancy location. The phenomenon of oxygen molecule adsorption at the S vacancy site is characterized by a robust bonding interaction. This interaction results in the introduction of p-type doping in  $\text{MoS}_2$ , leading to a conversion from trion to exciton. In addition, the application of strong oxygen plasma treatment on mechanically exfoliated  $\text{MoS}_2$  was observed. It can be used to modify the photoluminescence (PL) intensity, ranging from significantly high to complete reduction, depending on the duration of exposure. In Figure 2.8, the photoluminescence during plasma exposure from 1 s to 6 s is labeled as t1 to t6. The PL intensity decreases with increasing time of plasma exposure. The A exciton and B exciton were quenched after 3 s of plasma exposure. The observed behavior can be attributed to the change from direct to indirect bandgap because of the creation of defects that created by oxygen bombardment in the  $\text{MoS}_2$  (Kang et al., 2014).

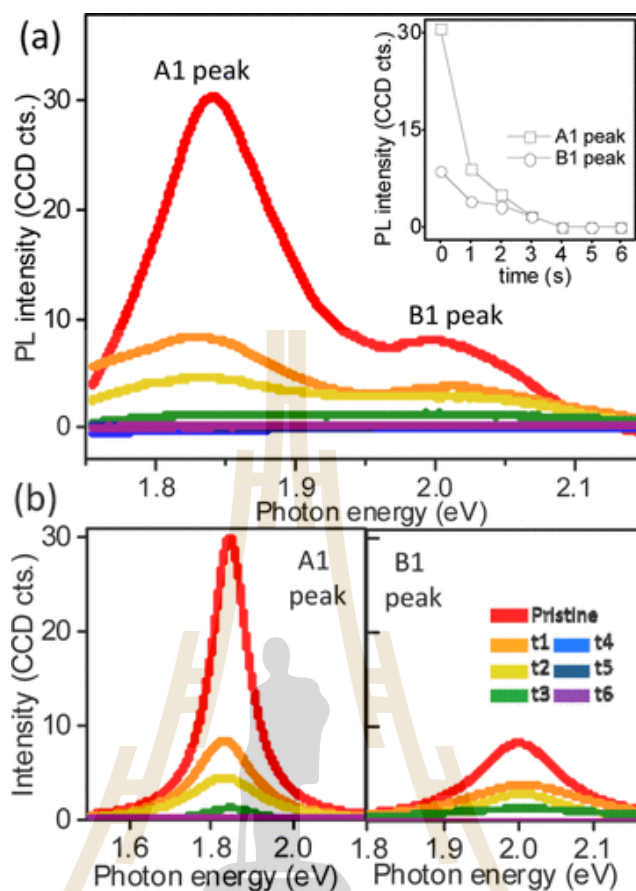


**Figure 2.8** (a) Time-dependent photoluminescence (PL) spectra of plasma-treated monolayer  $\text{MoS}_2$ . Inset shows the PL intensity of A and B peaks with respect to the plasma exposure time from 1 s to 6 s. (b) Corresponding to A and B excitons, the peaks in PL spectra were fitted with Lorentzian functions (Kang et al., 2014).

Another work, the modulation of photoluminescence (PL) by laser irradiation is attributed to structural damage caused by the laser, along with the subsequent adsorption of oxygen on the sample's surface under ambient conditions.

Three distinct behaviors were observed based on the duration of laser irradiation. These behaviors include slow photo-oxidation during the initial stage, where the intensity of photoluminescence (PL) slowly increases due to the physisorption of ambient gases. Then, fast photo-oxidation occurs during a later stage, leading to an increase in PL intensity because of chemisorption. Finally, photo quenching occurs, resulting in a reduction of PL intensity. The structural disorder is induced during the rapid photo-oxidation stage, leading to severe structural degradation during the

subsequent photo quenching stage. The role of oxidation is confirmed by conducting additional experiments in a vacuum, where the photoluminescence (PL) intensity decreases due to structural degradation without the involvement of oxygen functional groups. The impact of oxidation on charge scattering is further explained by observing the appearance and disappearance of neutral excitons and multiexcitons during each stage (Ho et al., 2016).

## 2.4 Electron irradiation

Electron irradiation can cause several types of structural defects due to atom displacement within the specimen or atom sputtering from the specimen. The amount of damage and defects caused by radiation is directly related to the amount of electron dose (Najmaei et al., 2013). The type of defect created is determined by the amount of energy transferred during irradiation, which is directly proportional to the accelerating voltage. In the case of MoS<sub>2</sub>, chalcogen vacancies can be created with an electron beam with a higher energy than knock-on threshold (80 kV for S atoms) (Komsa et al., 2013). Also, an accelerating voltage (>80 kV) in TEM can even create nanopores or cause defects to agglomerate in MoS<sub>2</sub> by direct sputtering of chalcogen atoms (Pakin et al., 2016). Therefore, low accelerating voltage (<10 kV) in an SEM that are numerous recent reports of defect formation below the knock-on voltage, but the underlying physical mechanisms remain unclear. One proposed mechanism for the formation of defects involves the localization of electrical excitation to emerging defect sites, which subsequently leads to a reduction in the displacement threshold energy required for vacancy formation (Lui et al., 2014). Jian-An et al. studied electron irradiation with an energy of 1 keV, followed by annealing, led to the creation of nanopores, cause by carbonaceous contaminant decrease in activation energy for defect creation (Jian-An et al., 2019). On the other hand, Pakin et al. reported the absence of interaction of carbonaceous contaminants with the sample (Pakin et al., 2016). Yagodkin et al. further demonstrated the formation of new charge-transfer excitons between carbonaceous contaminants and the MoS<sub>2</sub> sample (Yagodkin et al., 2022). Another work, Parkin studied the effect of electron beam induced sulfur vacancies on the first-order Raman modes was investigated. And the resulting effects

are analyzed in relation to the changes observed in the in-situ transmission electron microscopy two-terminal conductivity of monolayer MoS<sub>2</sub> during electron irradiation. They observed a red shift in the E' (in-plane mode vibration) peak and a less pronounced blue-shift in the A<sub>1g</sub> (out-plane mode vibration) peak with increasing electron dose. The removal of sulfur induced by electron irradiation is observed, and the correlation between the shifts in Raman peaks and the density of sulfur vacancies (which is on the order of a few percent) is shown in Figure 2.9. The intrinsic characteristics of defective systems include frequency shifts that correspond to changes in vacancy concentration (Parkin et al., 2016).

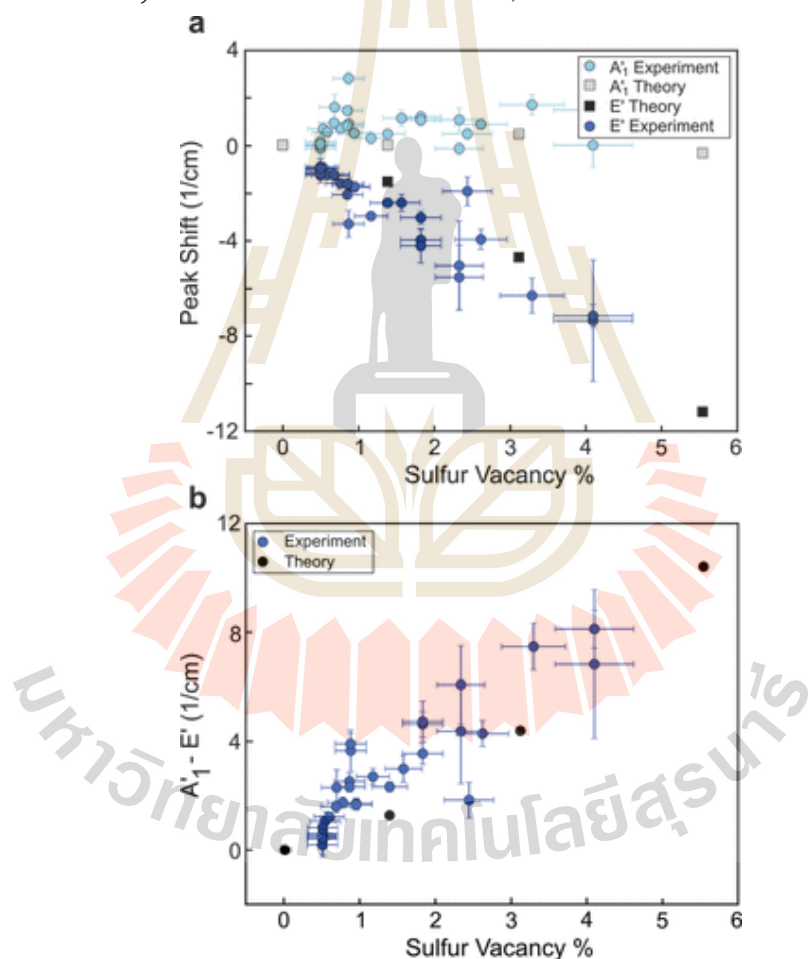


**Figure 2.9** Raman peak shift vs S vacancy: experiment and theory. (a) Experimental and theoretical individual peak shifts of the E' and A<sub>1g</sub> modes as a function of sulfur vacancy percentage. (b) Change in separation between the E' and A<sub>1g</sub> Raman modes as a function of defect concentration (Parkin et al., 2016).

## 2.5 Vibrational properties of TMDs.

Ab initio calculations have been employed to determine the phonon dispersions of both MoS<sub>2</sub> and WS<sub>2</sub>. The calculated phonon dispersion of MoS<sub>2</sub> was further compared and correlated with experimental Raman spectra, providing valuable insights into the vibrational properties of this material. The main Raman peaks correspond to the in-plane E' and the out-of-plane A<sub>1g</sub> mode are shown in Figure 2.10.

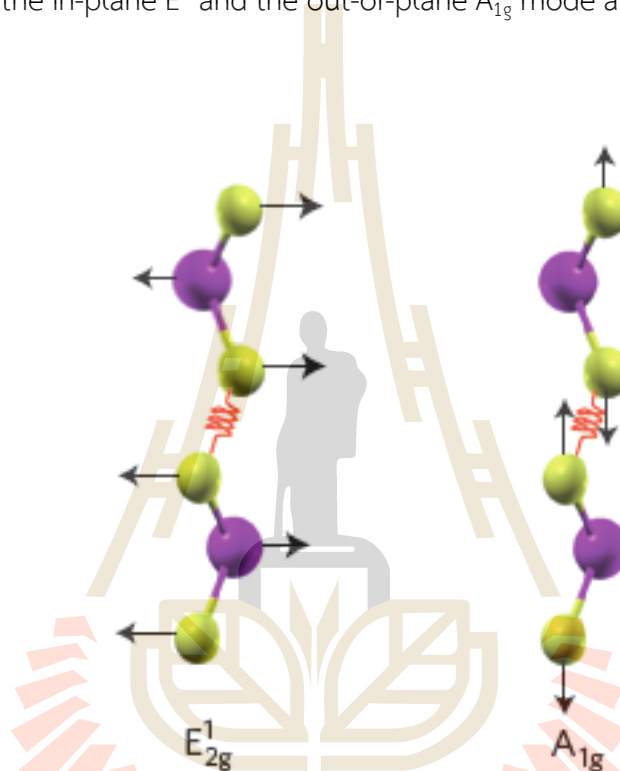


**Figure 2.10** Schematic representation of the in-plane phonon modes E' and the out-of-plane phonon mode A<sub>1g</sub> for the bulk MoS<sub>2</sub> (Molina-Sánchez et al., 2011).

Lee was studying when the layer thickness is reduced, the A<sub>1g</sub> mode located around 406.0 cm<sup>-1</sup> experiences a decrease in frequency, while the E' mode around 382.0 cm<sup>-1</sup> exhibits an increase is shown in Figure 2.11. Such changes in peak positions offer valuable insights for layer thickness identification using Raman spectroscopy. The underlying causes of these shifts have been attributed to the influence of neighboring layers on the effective restoring forces acting on atoms and the increased dielectric screening of long-range Coulomb interactions. These findings shed light on the fundamental mechanisms responsible for the observed Raman spectral changes in



layered materials as a function of their thickness (Lee et al., 2011).

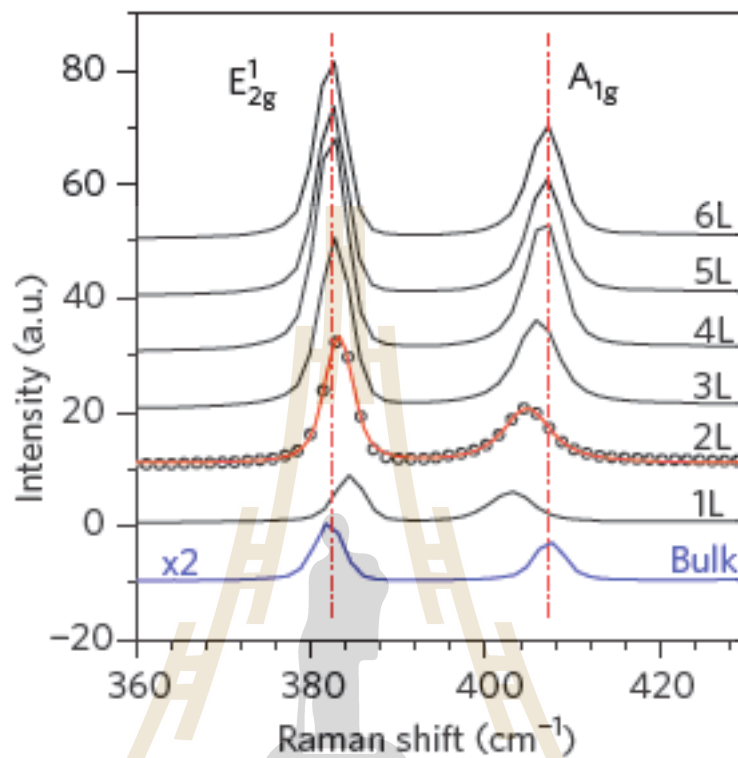


**Figure 2.11** Thickness-dependent Raman spectra for MoS<sub>2</sub>. The solid line for the bilayer spectrum is a double Voigt fit through data. The E' vibration shows slightly red shifts, while the A'₁g vibration shows slightly blue shifts with increasing sample thickness (Lee et al., 2011).

มหาวิทยาลัยเทคโนโลยีสุรนารี

## CHAPTER III

### METHODOLOGY

In this chapter, we will describe the process of electron irradiation by scanning electron microscopes (SEM), measuring techniques including confocal microscopy, Raman spectroscopy, and photoluminescence spectroscopy under  $N_2$  and ambient.

#### 3.1 Electron beam irradiation preparation

Electron beam irradiation is well known as an experimental method to modify the surface. Electron beam transfers energy to the sample by elastic and inelastic scattering mechanism that includes of sputtering, radiolysis, and can also lead to carbonaceous contamination. In this thesis, we investigate the modified surface in monolayer  $MoS_2$  using electron beam irradiation at ultralow accelerating voltages (5 kV) by field emission scanning electron microscope (FESEM), as shown in Figure 3.1. Scanning electron microscopy (SEM) operates by using a field-emission cathode in the electron gun to produce focused high-energy electron beams. The primary electron beam interacts with the sample surface and transfer energy to the sample.

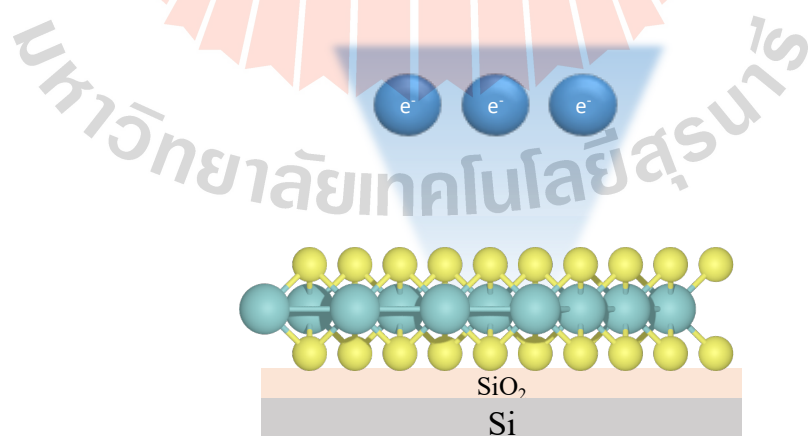


**Figure 3.1** Schematics of electron beam irradiation on monolayer  $MoS_2$  by SEM at ultralow energy with 5 kV accelerating voltage.

In this thesis, electron beam irradiation was performed in a Zeiss model Auriga. The electron dose was varied by scanning regions for different times while fixed accelerating voltage at 5 kV and specimen current at 265 pA. The electron dose (D) of irradiation was calculated by the number of electrons that received per unit area, given by  $e^-$  dose =  $\frac{I \times t}{A}$ , where I, t and A, stand for current, total irradiation time, and area scanned on the sample, respectively. In a scanning electron microscope (SEM), the electron dose can be varied by changing t, or A. In our experiment, we varied the total irradiation time while keeping the current (I) and the scanned area (A) on the sample constant to adjust the electron dose.

### 3.2 Confocal microscopy

Confocal microscopes have the capability to perform three-dimensional imaging that combined from each of individual layer. Hence, confocal microscopes are suitable for studying thin films. This is achieved by spatially filtering both the excitation source and the detector to converge at a common focal point. Confocal microscopy is based on the fundamental principle of focusing the illumination and detection optics on the same diffraction-limited spot. This spot is then systematically scanned over the sample, which is moved over the sample to create the image in the detector. We start by setting up a confocal microscope, the schematic of which is shown in Figure 3.2.

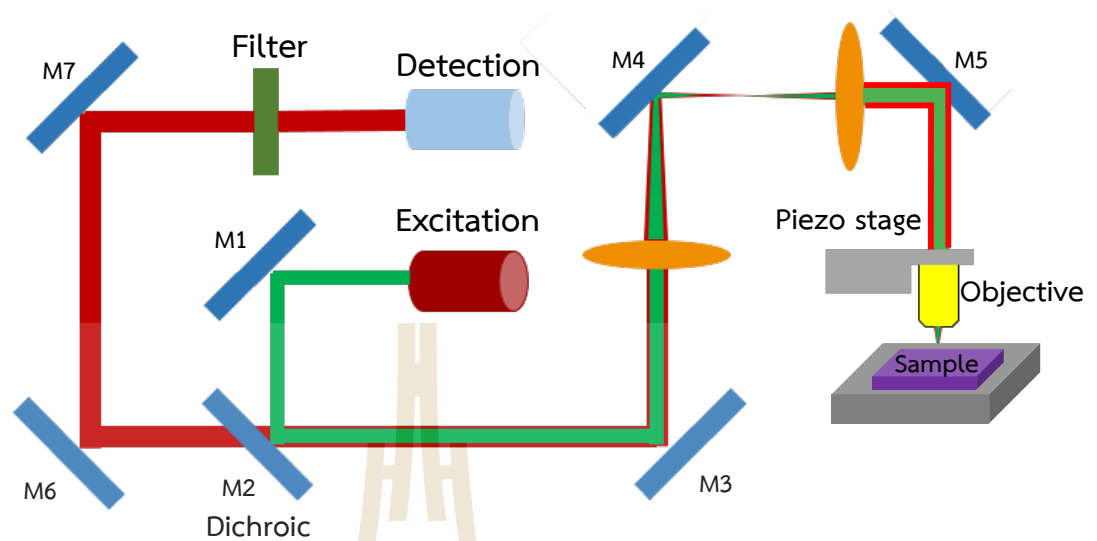


**Figure 3.2** Diagram of a confocal microscope setup.

The excitation source with a wavelength of 532 nm (Coherent OBIS 532) is aligned to the sample by following the green path shown in the image. M in the diagram refers to a mirror (Thorlabs BB1-E02). Then, it was reflected from a dichroic mirror (DMLP567) to the XY-axis galvo mirrors to scan the sample in two directions (x-y plane). After that, the light passes through the galvo and the lenses (L1 and L2) onto the objective lens. At the position in front of the sample, we install the 100x objective lens (Olympus MPLanFL N 100x) to focus the light beam onto the sample. The piezo stage enables scanning in the z-direction and fine-tuning of the confocal image. The sample is positioned at the focal point of the objective lens. When the sample is excited, fluorescence light in the range above 600 nm is collected through the dichroic mirror (DMLP567), which allows the transmission of light with wavelengths greater than 567 nm. Finally, the signals are divided into two parts using a fiber beam splitter for intensity measurements with an avalanche photodiode detector (APD), and for spectrum analysis with a spectrometer (Andor DU940P-BU2, 300  $\mu$ m grating, Kymera 328i CCD). The longpass filter is removed during the spectrum analysis.

### 3.3 Raman spectroscopy

Raman spectroscopy is a widely used spectroscopic technique used to study the vibrations and rotations of molecules, as well as other phenomena such as lattice phonons and electronic transitions. It is based on the scattering of monochromatic light, typically from a laser source, by a sample. When light is scattered by a sample, a small fraction of the photons is scattered inelastically. This energy shift is characteristic of the vibrational modes of the sample. Therefore, Raman spectra is a characterization method for studying the evolution of structural parameters in layered materials, providing insights into the transition from 3D bulk to 2D van der Waals bonded structures. It has become popular for determining the number of layers in layered materials. Generally, two prominent Raman peaks,  $E'$  (in-plane vibration) and  $A_{1g}$  (out of plane vibration) are commonly analyzed to gain insights into the crystal structure of  $\text{MoS}_2$ . During the transition from bulk to monolayer, two observed trends can be obtained: the  $E'$  peak shows a blue shift and the  $A_{1g}$  peak shows a slightly red shift, resulting in a difference between the two peaks of around  $19.0 \text{ cm}^{-1}$ . In this thesis, Raman measurements were achieved by SENTERRA II Dispersive from Bruker Optics, as shown in Figure 3.3. under ambient conditions. The excitation laser wavelength with 532 nm and power 50 mW with 100x objective, and 1200 gr/mm grating was used to perform spectra imaging. Typically, two Raman peaks,  $E'$  and  $A_{1g}$ , are commonly investigated to reflect the crystal structure of  $\text{MoS}_2$  corresponding to the in-plane and

out-of-plane vibration modes, respectively. Raman spectra were characterized, and we focused on Raman frequency that analyzed by 2 Voigt peaks (Gaussian and Lorentzian).



**Figure 3.3** SENTERRA II Dispersive Raman Microscope from Bruker Optics.

### 3.4 The photoluminescence spectroscopy under $N_2$

We can hypothesize that the recovery of photoluminescence (PL) intensity arises from the nitrogen and oxygen molecules that present in the ambient air. To better understand the recovery of PL intensity under ambient air, we did the experiment in both  $N_2$  gas and ambient air. Our methodology, we enclosed the sample within a box and continuously flowing nitrogen over it for a duration of 10 hours. During this period, we controlled the outlet pressure at 16 psi for the first hour and then kept a constant flow at 12 psi for the remaining 10 hours. Subsequently, we transitioned the conditions to ambient air, as shown in Figure 3.4 and Figure 3.5.

And then the high-power laser with 532 nm at 14.7 mW was exposed to our sample for 10 s. The dark spot on the sample was observed. After that, we changed the condition by venting. We measured the PL image and spectrum of our sample in the ambient air for 10 hours.



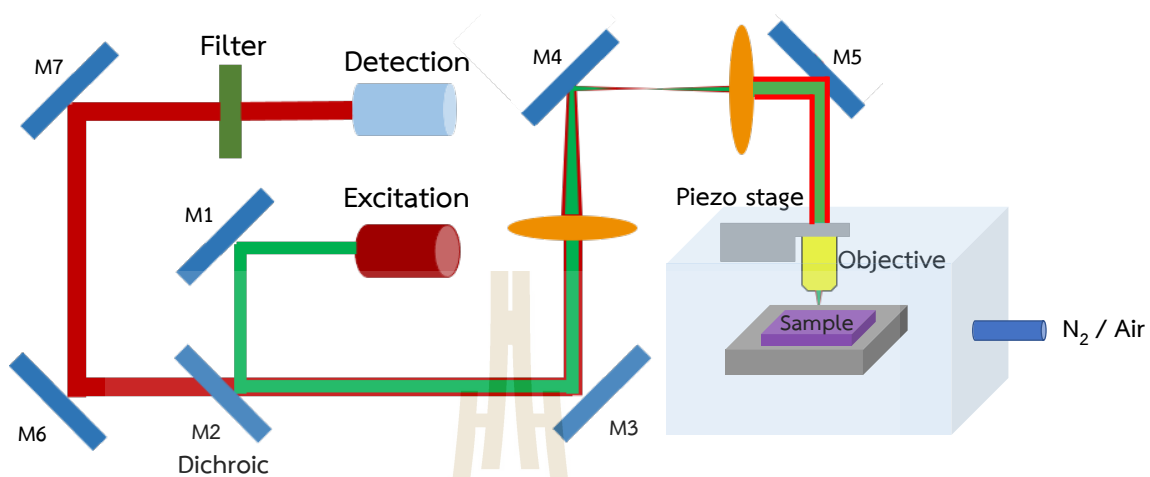


Figure 3.4 Diagram of a confocal microscope setup under  $N_2$  and ambient.

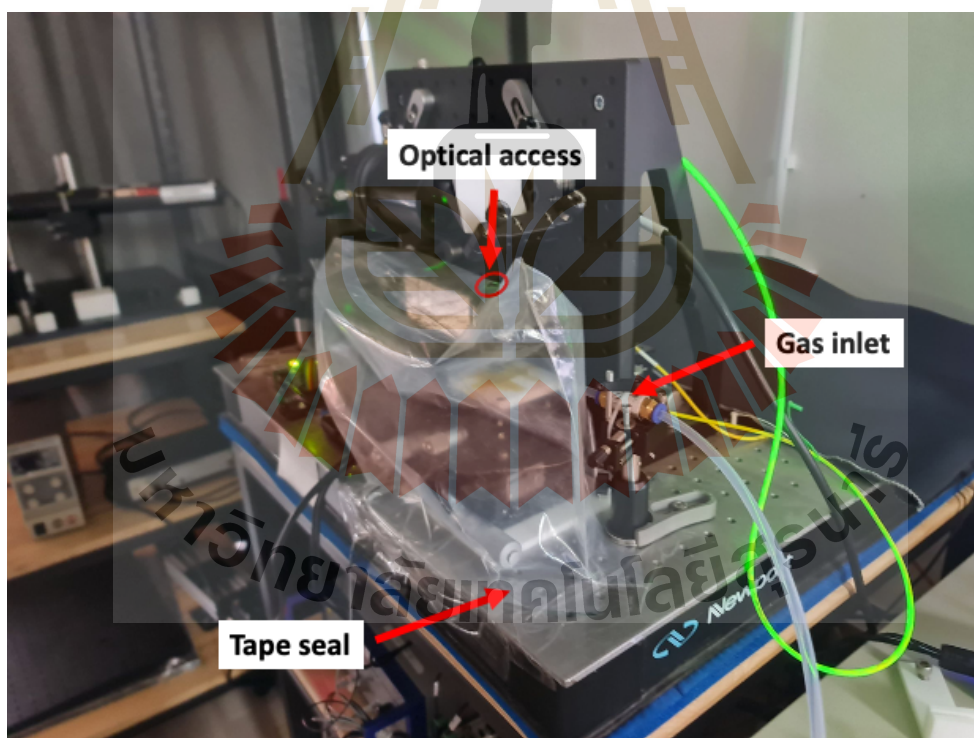
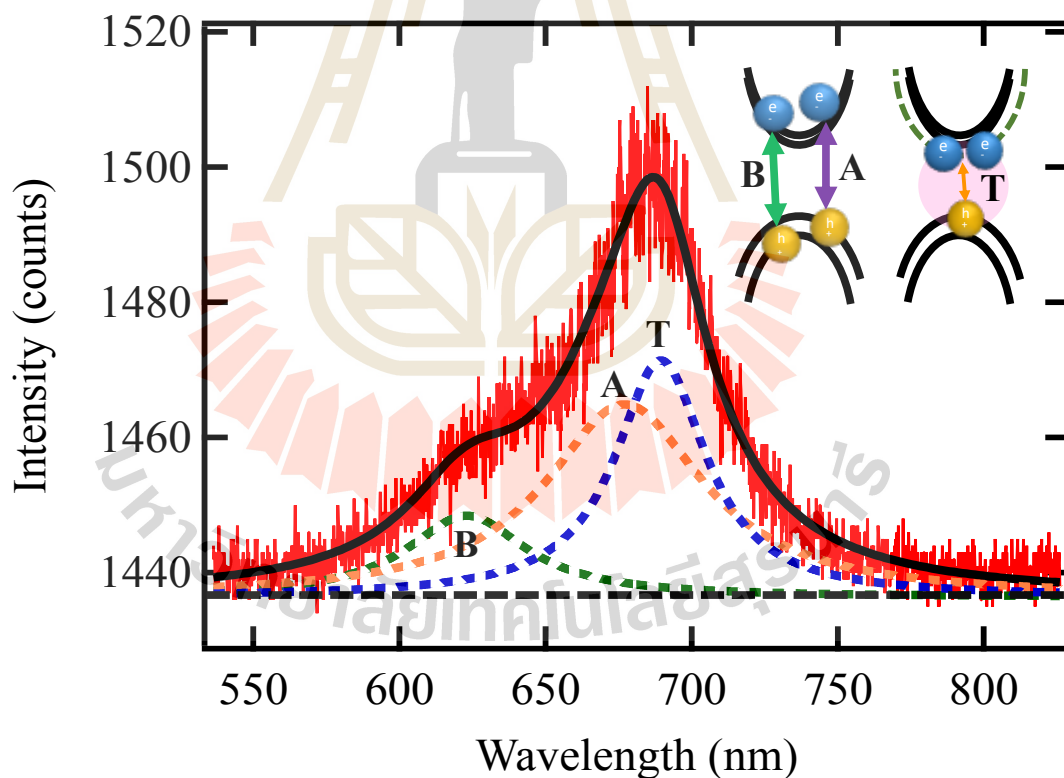


Figure 3.5 The experiment setup.

### 3.5 Processed photoluminescence data

The emission of light from a material by photo excitation is known as photoluminescence (PL). The photoluminescence spectra are a representation of the intensity of emitted light as a function of wavelength. It is obtained by integrating the intensity over a narrow wavelength range. The photoluminescence data from the experiment are pre-processed (raw data) and obtained from the spectrometer (Andor, DU940P-BU2). The photoluminescence data of monolayer MoS<sub>2</sub> was fitted with three Lorentzian functions corresponding to the A exciton, the B exciton from the spin orbit splitting, and the trion high-wavelength tail length from when either an electron or a hole bind to an exciton as presented in Figure 3.6.



**Figure 3.6** Three Lorentzian functions consisting of A exciton, B exciton, and trion peak were fitted to the unprocessed photoluminescence data of monolayer MoS<sub>2</sub>. Inset: Band structure diagram for A exciton, B exciton and trion.

From fitting the data with 3 Lorentzian functions, we can obtain the constants representing the background contribution present in the intensity that are shown in the back dash line in Figure 3.5. This background arises from various instrumental effects, such as detector noise or instrument resolution. Subtracting a constant from the data does not change the significant features of the photoluminescence (PL) spectrum. This process removes any baseline offset or background signal that might be show in the data. By performing this operation, the essential characteristics and important information contained in the PL spectrum remain unchanged and unaffected. Subsequently, the subtracted data was normalized by dividing each data point by its maximum value. This normalization technique scales the entire dataset, showing that all values within a range of 0 to 1. By normalizing in this process, the relative intensity values are preserved, facilitating meaningful comparisons and interpretations of the data across different measurements. The normalized data is shown in Figure 3.7.

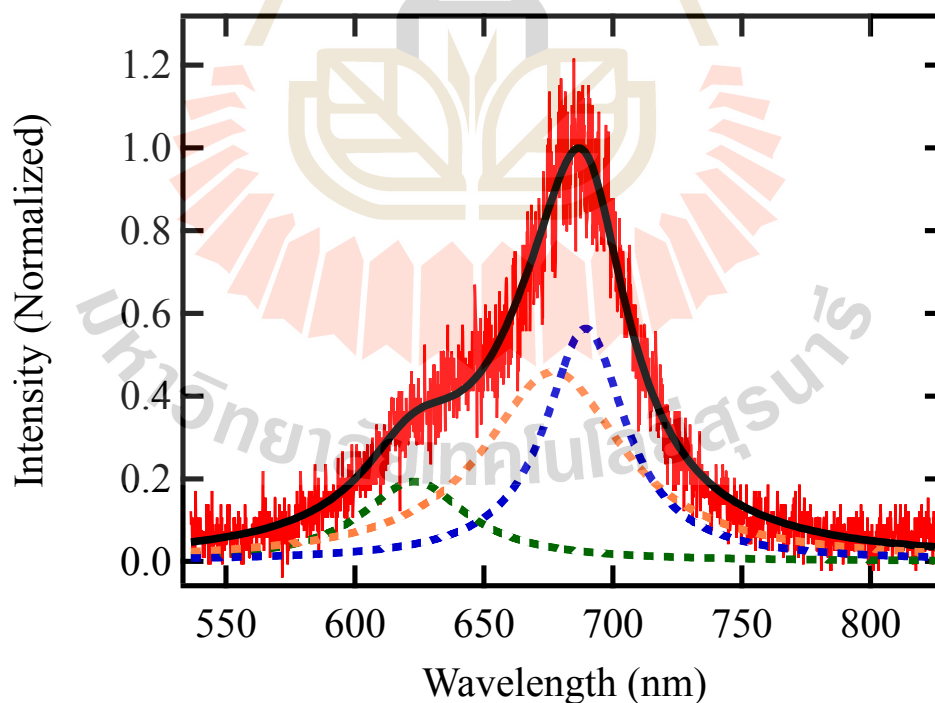


Figure 3.6 The normalized data after subtracting data by constant background.

## CHAPTER IV

### RESULTS AND DISCUSSION

This chapter presents the results and the discussion. The contents consist of the photoluminescence image of sample which describes the morphology electron irradiated areas. The photoluminescence spectrum and Raman spectrum that describes the characteristic and mechanism of sample. The last content on this chapter is a discussion that will reveal the cause of the recovery of photoluminescence after high power laser expose and store in the ambient air.

#### 4.1 Photoluminescence spectroscopy observation

The sample was characterized using optical spectroscopic technique to determine the structure and chemical properties of monolayer MoS<sub>2</sub>. Firstly, the monolayer MoS<sub>2</sub> was purchased from 2D Semiconductors, USA. This hexagonal phase, undoped monolayer MoS<sub>2</sub> was prepared on a SiO<sub>2</sub>/Si substrate using atmospheric pressure chemical vapor deposition (APCVD). Actually, the number of layers is confirmed using photoluminescence and Raman spectroscopy. For pristine monolayer MoS<sub>2</sub>, the PL spectrum in Figure 4.1 was observed and fitted with 3 Lorentzian peaks, comprising 3 components. The A exciton peak at 677 nm (blue dashed line) and the B exciton peak at 623 nm (green dashed line) arise from spin-orbit splitting of the valence band. The trion which is a quasiparticle consisting of 2 electrons and 1 hole (Mak et al., 2012), appears at a high wavelength tail length of 690 nm (light blue dashed line). The optical band gap of 677 nm observed in Figure 4.1 confirms the monolayer thickness of the sample (Mak et al., 2011). Moreover, we observed the photoluminescence (PL) images using a fixed power laser at 118  $\mu$ W to avoid damage to the sample.

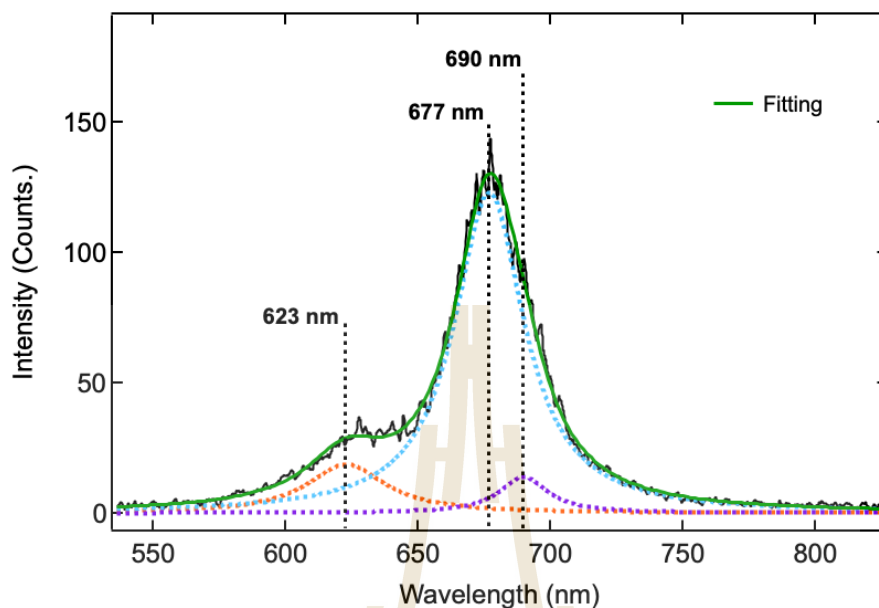


**Figure 4.1** The PL spectrum of pristine monolayer  $\text{MoS}_2$  consists of three components: an A exciton (A) peak at 677 nm, a B exciton (B) peak at 623 nm, and a trion (T) peak at 690 nm.

The PL image was obtained at the focus point using a home-built confocal microscope setup showing the uniformity of the sample and some cracks line on the surface. However, the 8 points of this area that we randomly picked show qualitatively similar PL spectra, as shown in Figure 4.2.

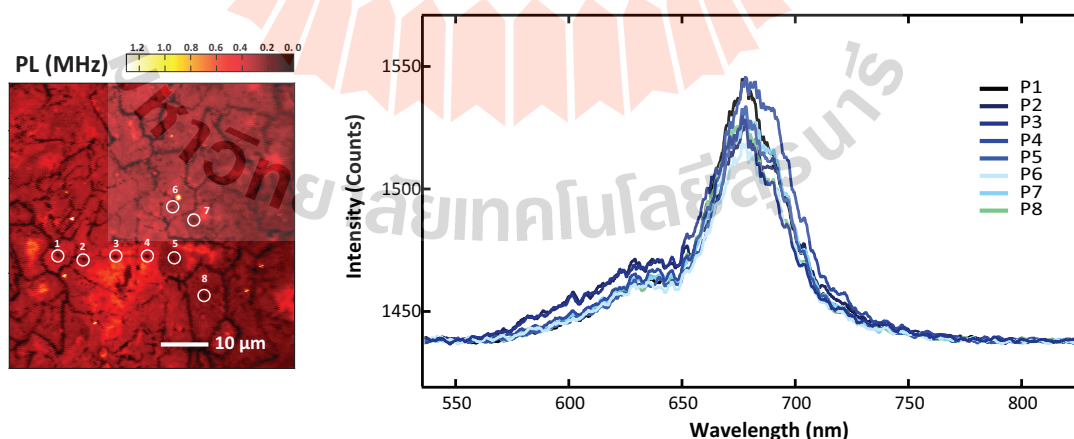


**Figure 4.2** (Left) The confocal PL intensity image of pristine monolayer  $\text{MoS}_2$  and (Right) the PL spectra of each point on the pristine monolayer  $\text{MoS}_2$ .

After that, the monolayer MoS<sub>2</sub> sample was irradiated with electron beam on the surface at different regions. The accelerating voltage was fixed at a low voltage of 5 kV to avoid generation of additional defects. Two different electron doses of  $D = 0.3 \times 10^3 \mu\text{C}/\text{cm}^2$ , and  $D = 5.3 \times 10^3 \mu\text{C}/\text{cm}^2$  were used to investigate the effect of the dose on the PL properties and are referred to as the low electron dose and high electron dose, as shown in Figure 4.3.

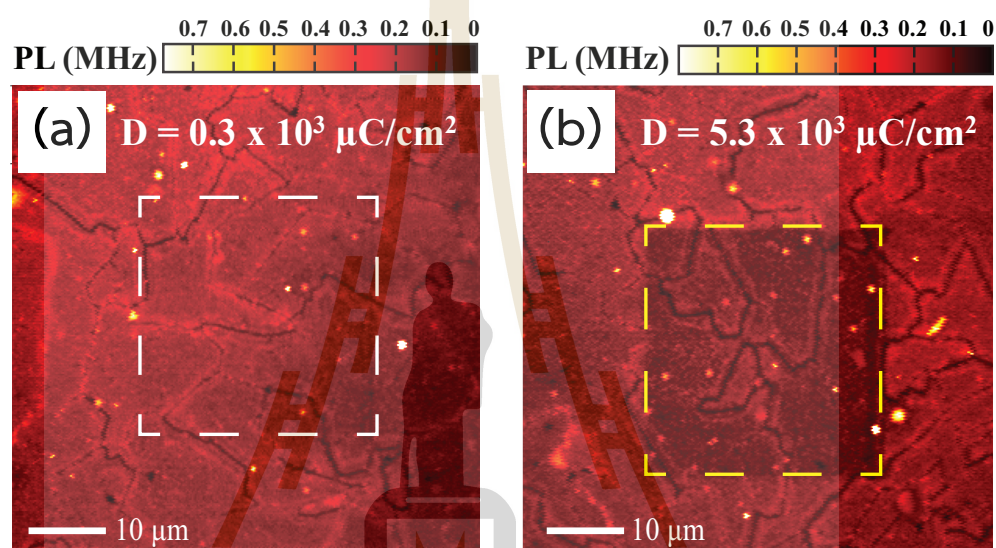


**Figure 4.3** Confocal PL intensity image of the irradiated sample showing e-beam irradiated regions by SEM at 5 kV accelerating voltage corresponds to (a) an electron dose of  $0.3 \times 10^3 \mu\text{C}/\text{cm}^2$  (white box) and (b)  $5.3 \times 10^3 \mu\text{C}/\text{cm}^2$  (yellow box), respectively.

We can observe that the photoluminescence intensity from the MoS<sub>2</sub> after low electron dose condition is the same as that of the surrounding pristine area. Another hand, we observed a photobleaching effect in the area exposed to a high electron dose. The photobleaching is a situation where the MoS<sub>2</sub> surface undergoes a permanent loss of fluorescence capability owing to chemical damage, resulting in a decrease in PL intensity (Demchenko et al., 2020).

In addition, after electron irradiation, we do not observe any shift in the PL spectra that has been previously associated with the generation of S vacancy, thus confirming that the structure remained unchanged after electron irradiation, as shown



in Figure 4.4. And we note that the lower intensity of the unnormalized PL spectra for high electron dose condition is attributed to photobleaching.

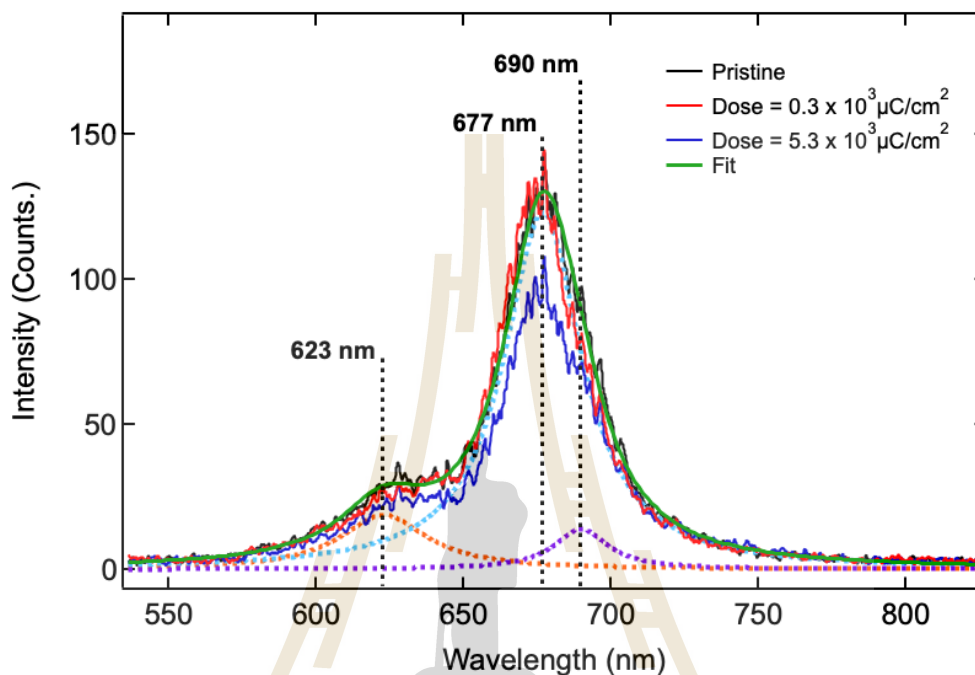


**Figure 4.4** Comparison of the PL spectrum of pristine (black line), electron irradiated dose of  $0.3 \times 10^3 \mu\text{C}/\text{cm}^2$  (red line) and  $5.3 \times 10^3 \mu\text{C}/\text{cm}^2$  (blue line), respectively. Each of spectrum comprises of 3 components: A exciton peak at 677 nm, B exciton peak at 623 nm and trion peak at 690 nm.

After that, a laser with 532 nm (14.7 mW) illuminated on the sample under ambient air. We found that the quenching area of PL intensity, as shown Figure 4.5.

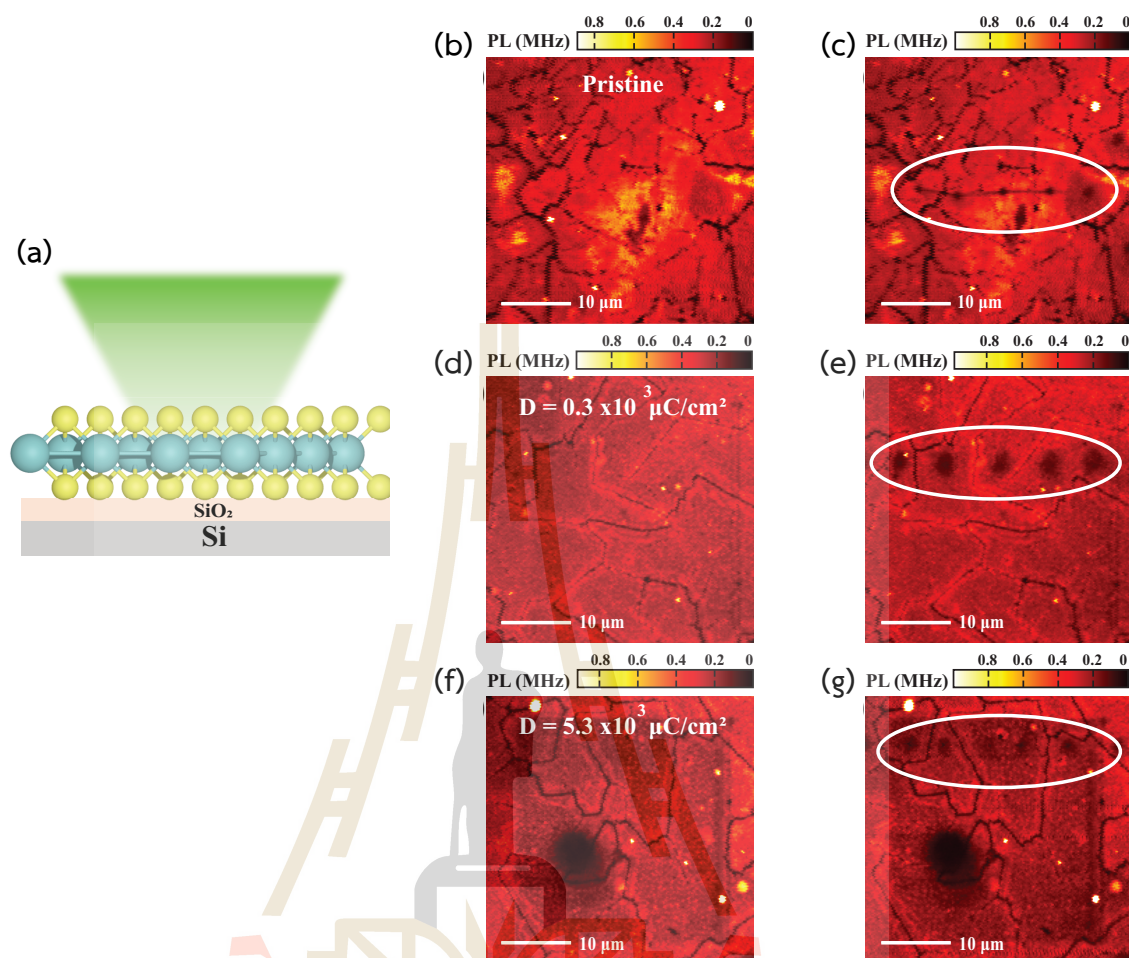


**Figure 4.5** a) Schematics of high-power laser exposure at 14.7 mW on monolayer MoS<sub>2</sub> under ambient. Confocal PL intensity image of pristine monolayer MoS<sub>2</sub> (b) before, and (c) after high power laser exposure for 10 s of the pristine MoS<sub>2</sub> (d) before, (e) after high power laser exposure for 10 s of the area that was irradiated electron dose  $0.3 \times 10^3 \mu\text{C}/\text{cm}^2$ . And the condition of electron irradiation dose  $5.3 \times 10^3 \mu\text{C}/\text{cm}^2$  (f) before, (g) after high power laser exposure for 10 s.

Then, after storing in ambient condition for 10 h, we observed an intriguing phenomenon that PL intensity can be recovery under the condition of a low electron dose. Another hand, the PL intensities of pristine and high electron dose condition remained quenched, as shown in Figure 4.6.

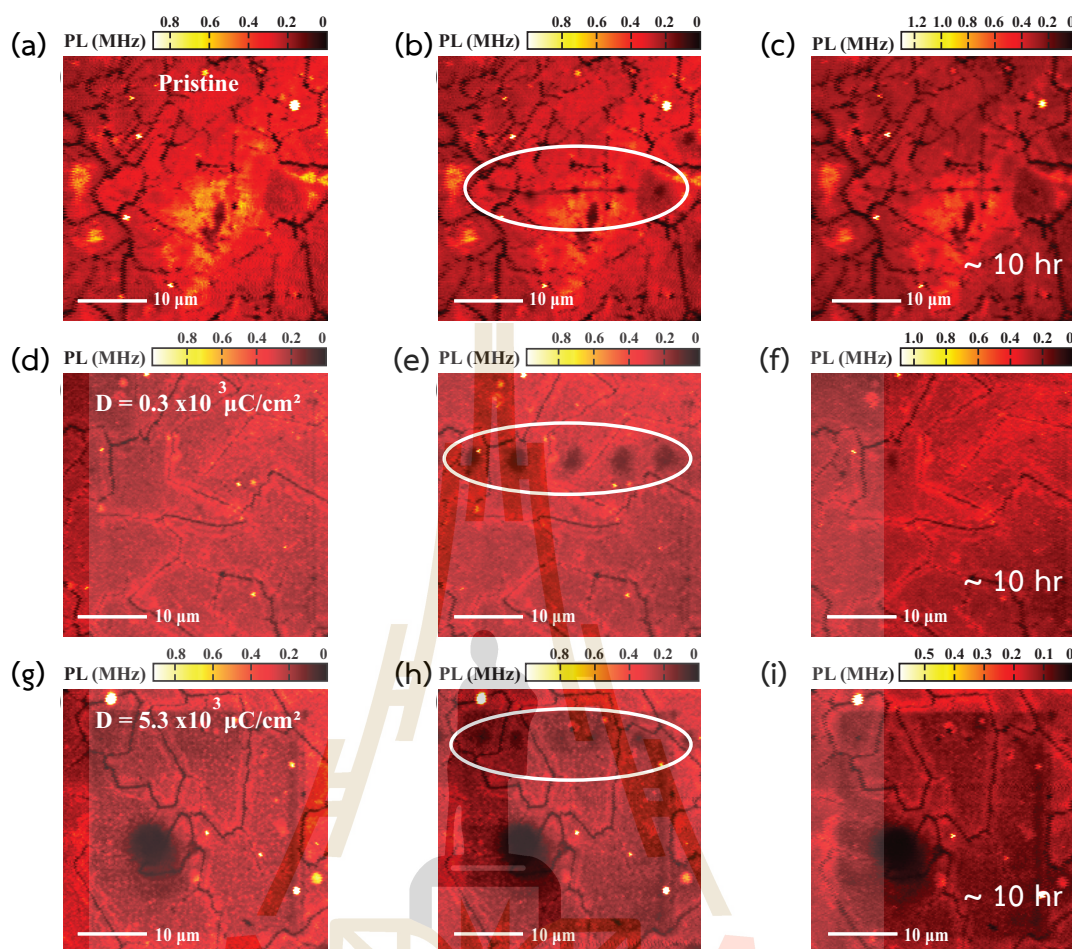


**Figure 4.6** Confocal PL intensity images of pristine monolayer MoS<sub>2</sub> (a) before, (b) after high power (14.7 mW) exposure for 10 s and (c) after storing in the ambient air for 10 hours. For the condition electron irradiation dose  $0.3 \times 10^3 \mu\text{C}/\text{cm}^2$  (d) before, (e) after high power (14.7 mW) exposure for 10 s and (f) after storing in the ambient air for 10 hours. And the electron irradiation dose  $5.3 \times 10^3 \mu\text{C}/\text{cm}^2$  (g) before, (h) after high power (14.7 mW) exposure for 10 s and (i) after storing in the ambient air for 10 hours.

To quantitatively study the recovery, relative PL intensity was calculated by dividing the PL intensity of the quenched area after exposure by the PL intensity of the same area prior to the exposure, as shown in Figure 4.7.

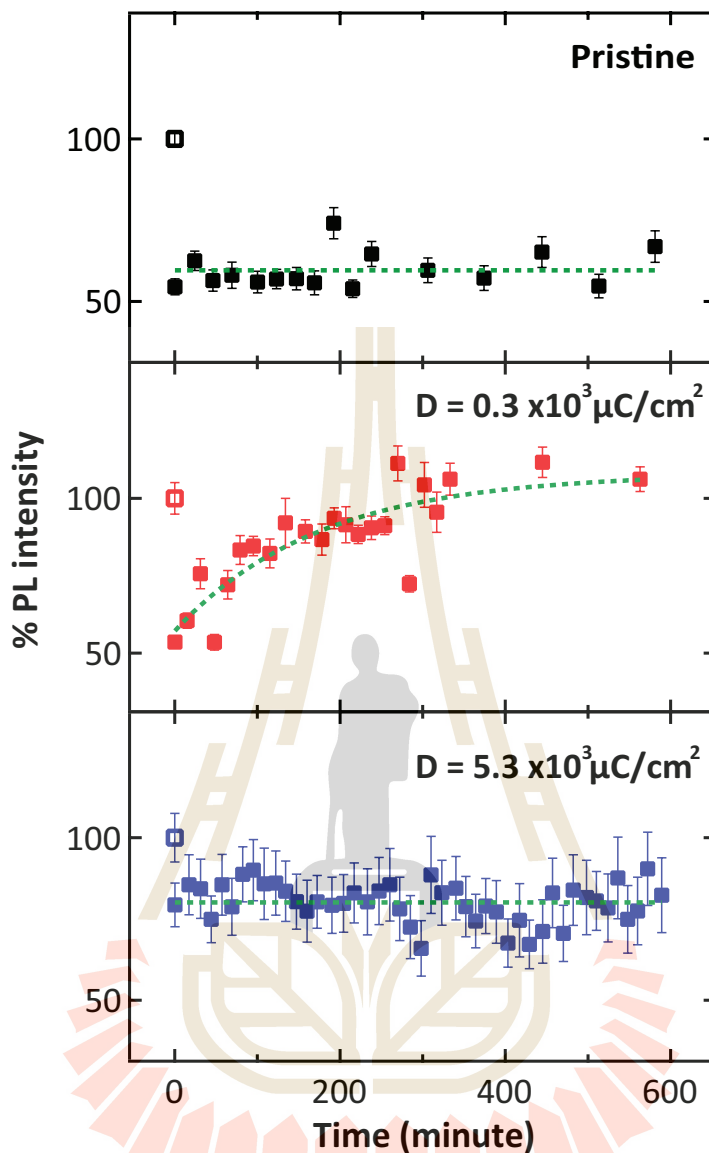


**Figure 4.7** The relative PL intensity with varying different condition consist of pristine, low electron dose, and high electron dose after high power exposure and storage in ambient air for 10 hours.

In the case of pristine sample, the relative PL intensity of the illuminated area decreased by 50%, and following ambient storage, there was no recovery of PL intensity (black square). We attribute this behavior to the lack of active site on the cleaned surface for gas adsorption.

Also, high electron dose condition, the original PL intensity of cannot be recovered, and the quenching area remained unchanged during ambient storage. We attribute this irreversibility to the photobleaching, which is also evidenced by the lower initial PL intensity (Oh et al., 2016).

On the other hand, the PL recovery can be observed in the case of low electron dose condition, where the PL intensity gradually increased to close to the original state after storing the sample in ambient condition for 10 hours. In this case, we hypothesize that the irradiation provides electronic charge on the surface of MoS<sub>2</sub>, which stimulated gas adsorption on the surface. Then, the charge transfer from the sample to the gas molecule can occur, leading to PL recovery.

To identify the gas species associated with the PL recovery mechanism, we further investigated the PL behavior of monolayer MoS<sub>2</sub> irradiated by low electron dose condition again in the N<sub>2</sub> atmosphere for 10 hours followed by an ambient storage for another 10 hours. According to PL spectra in Figure 4.8, a red shift was observed in PL spectrum after the exposure, and the shift remained unchanged during which the sample was kept in N<sub>2</sub> for 10 hours. On the other hand, the PL spectrum reverted to its original position after storing in ambient conditions for 10 hours.

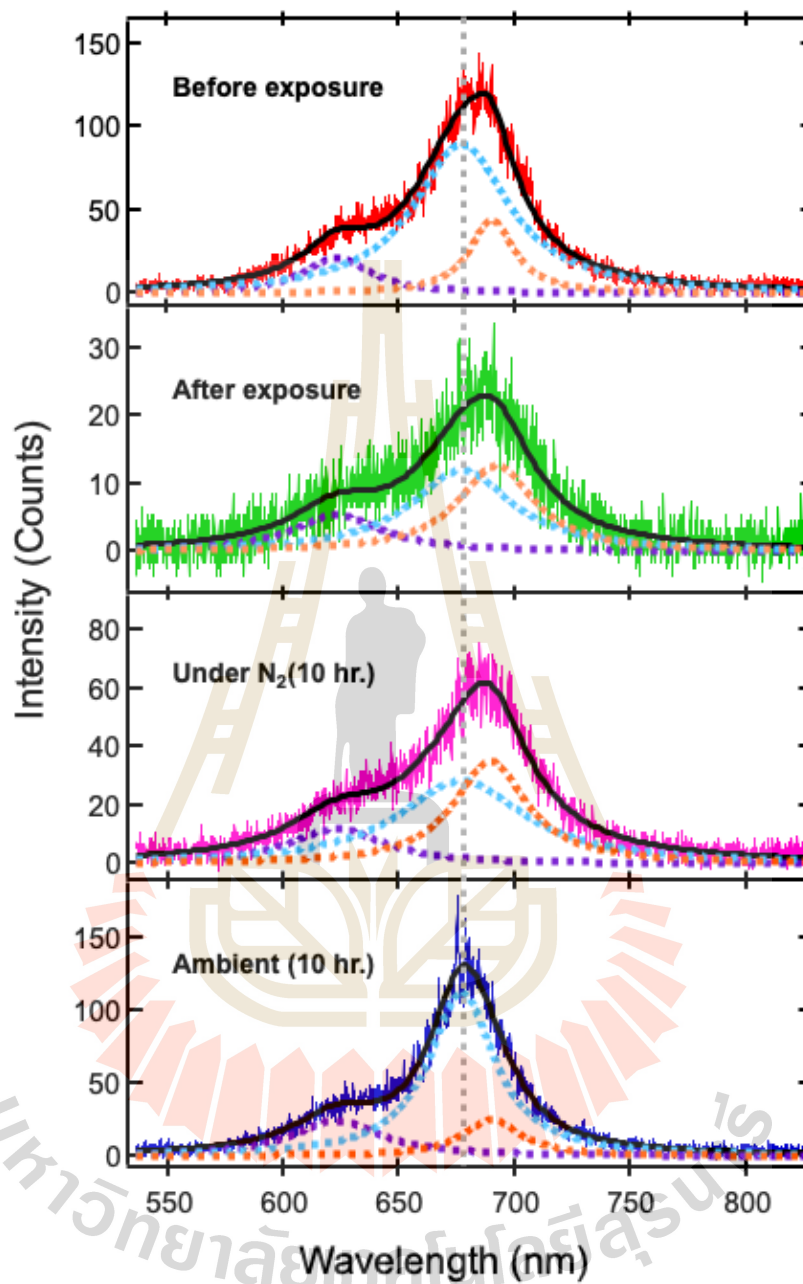


**Figure 4.8** The PL spectra of electron irradiation area consist of before high-power laser exposure, immediately after high power laser irradiation, after 10 hours storage under N<sub>2</sub> and after another 10 hours storage in ambient conditions represented by red line, green line, and pink line, and blue line respectively.



Moreover, the relative PL intensity of the exposed area decreased by 50% and remained unchanged under  $N_2$  atmosphere, as shown in Figure 4.9. Therefore, we can conclude that nitrogen gas ( $N_2$ ) does not affect the recovery of photoluminescence.

On the contrary, the PL intensity gradually increased in the subsequent exposure to ambient condition. This result suggests that the significant recovery of PL can be attributed to the physical adsorption of  $O_2$  molecules from the air (Figure 4.9).

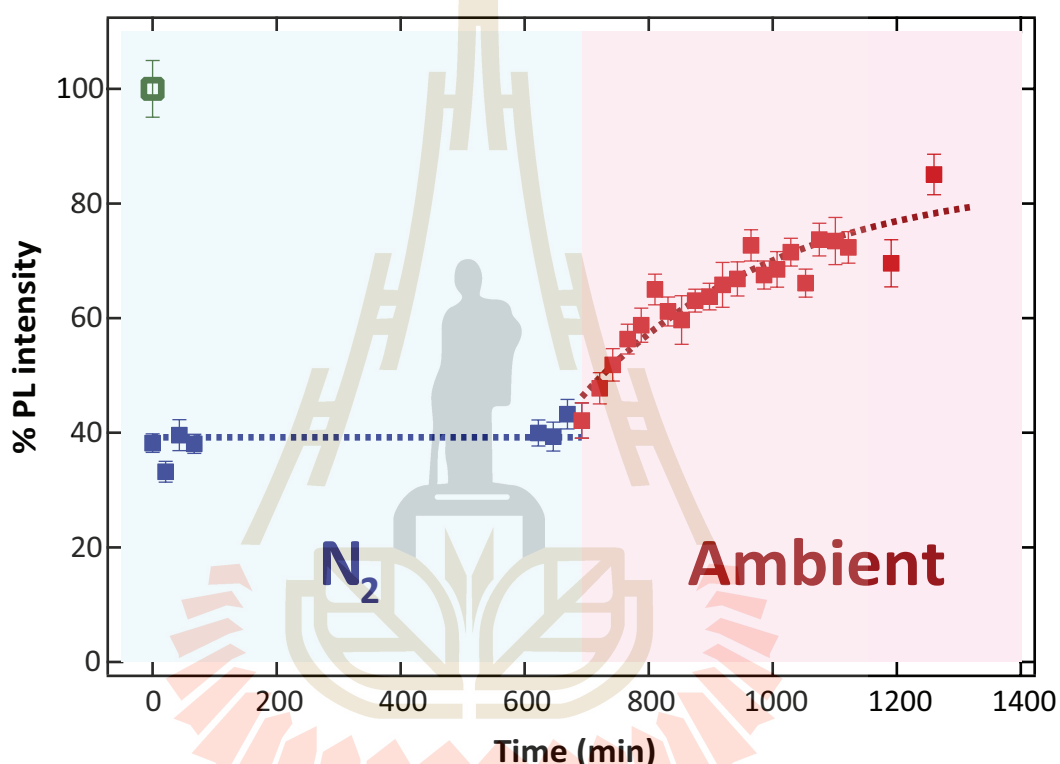
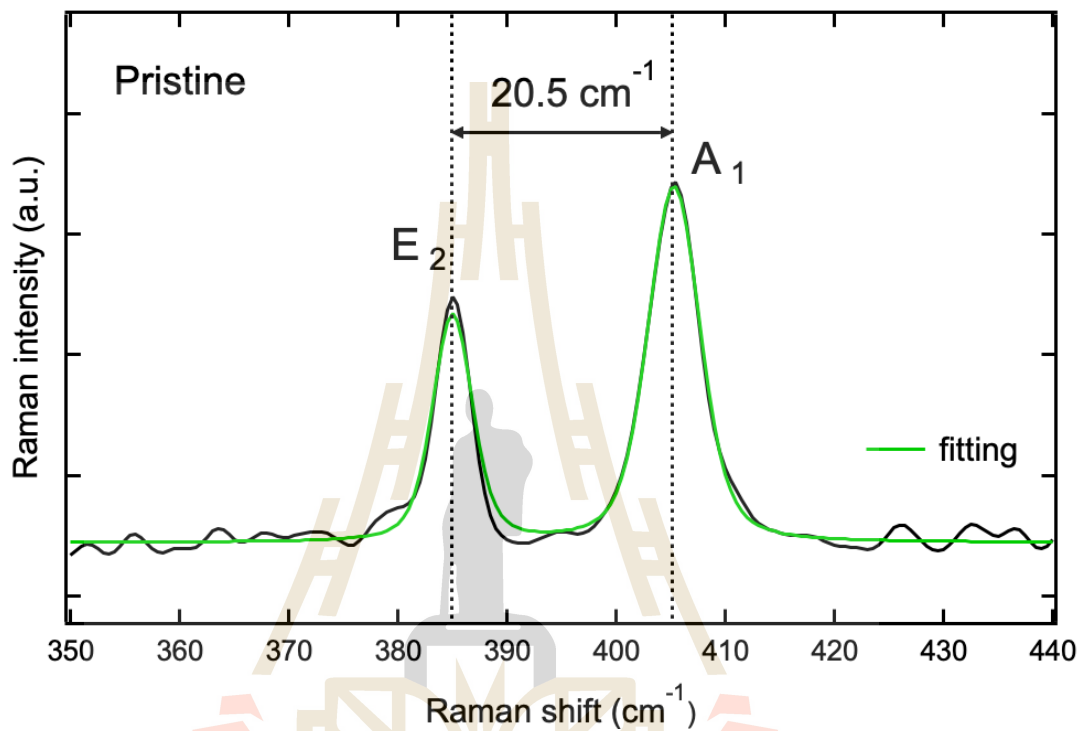


Figure 4.9 The PL intensity under  $N_2$  and ambient air.

## 4.2 Raman spectroscopy observation

Raman spectroscopy is a widely used characterization method that easily illustrates the evolution of structural in layered materials, during the transition from 3D bulk blocks to 2D van der Waals bonded structures. Typically, Raman spectroscopy is used to investigate defects such as S vacancy, which is created by electron irradiation. Moreover, it can be used to determine the number of layers and uniformity of monolayer  $MoS_2$  samples by evaluating the difference in energy of the vibrational modes. According to Raman spectra in Figure 4.10, the characteristic peaks appear at  $\sim 385\text{ cm}^{-1}$  and  $\sim 403\text{ cm}^{-1}$  corresponding to in-plane  $E_2$  mode and out-of-plane  $A_1$

mode, respectively. In addition, the peak positions for  $E_2$  and  $A_1$  modes were determined by fitting two Lorentzian functions to the spectra. The difference between these two modes is  $20.5\text{ cm}^{-1}$ , consistent with a monolayer  $\text{MoS}_2$  (Lee et al., 2011).



**Figure 4.10** The Raman spectrum of pristine of monolayer  $\text{MoS}_2$ . The left and right dashed line indicate the position of  $E_2$  and  $A_1$  peaks and position difference of  $20.5\text{ cm}^{-1}$  that confirming the monolayer  $\text{MoS}_2$ .

To better understand the mechanism of electron irradiation on sample, we recorded a series of Raman spectra of monolayer  $\text{MoS}_2$  irradiated at varying electron dose. We observe that the peak positions remained changed under both low and high electron dose conditions after electron irradiation compared to the pristine condition, as shown in Figure 4.11.

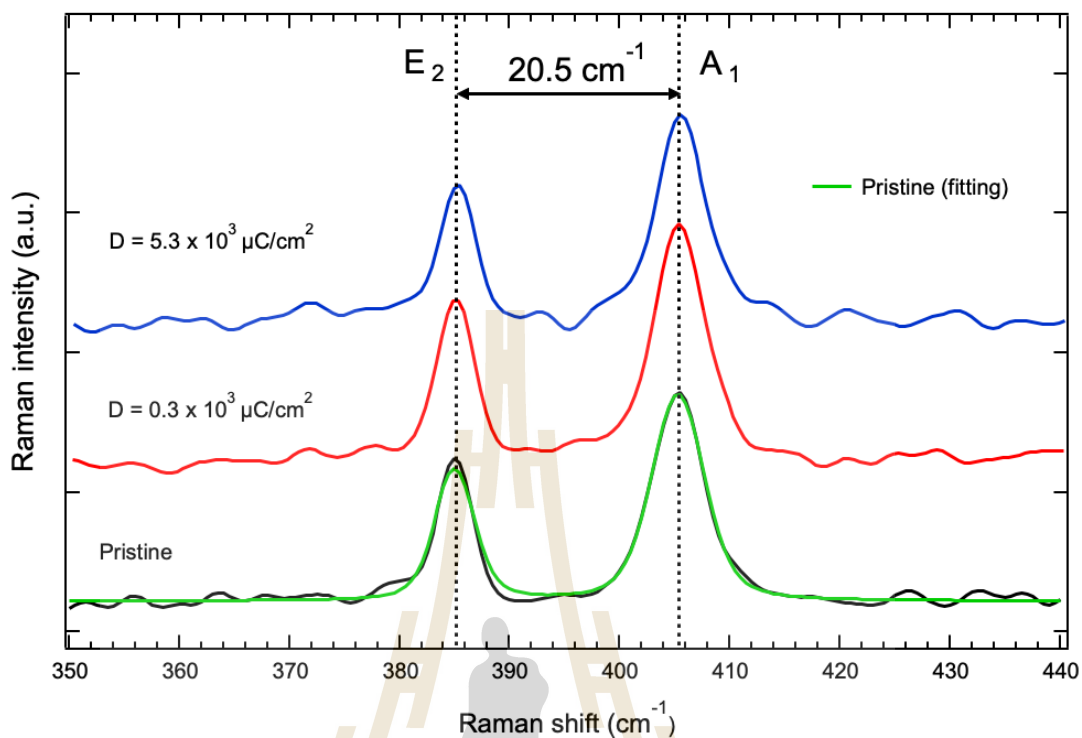


**Figure 4.11** Raman spectra of different conditions include of pristine (black line), electron irradiated dose of dose  $0.3 \times 10^3 \mu\text{C}/\text{cm}^2$  (red line) and dose  $5.3 \times 10^3 \mu\text{C}/\text{cm}^2$  (blue line) respectively.

Moreover, in the case of high electron dose irradiation dose, the position of  $A_1$  mode and  $E_2$  mode show a shift from  $405.3 \text{ cm}^{-1}$  to  $405.6 \text{ cm}^{-1}$  and from  $385.0 \text{ cm}^{-1}$  to  $385.2 \text{ cm}^{-1}$ , respectively. In the case of low electron dose, the position of  $A_1$  mode slightly shifts from pristine from  $405.3 \text{ cm}^{-1}$  to  $405.4 \text{ cm}^{-1}$  and remains unchanged for  $E_2$  mode, as shown in Figure 4.12.

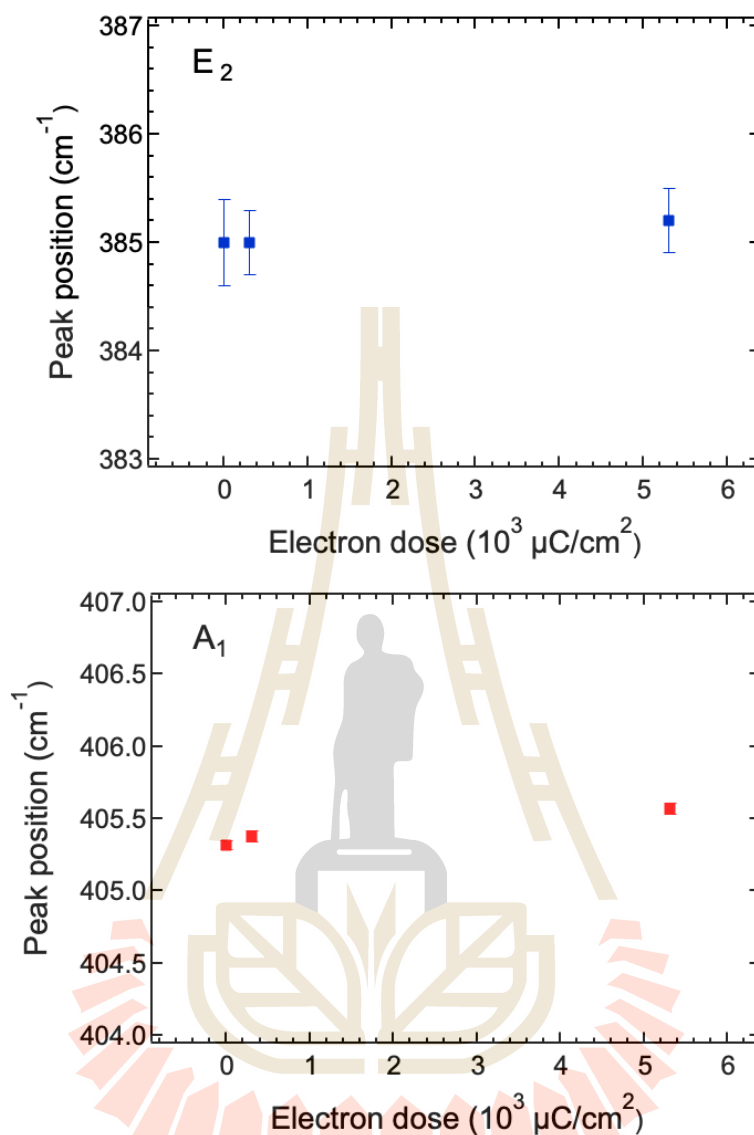
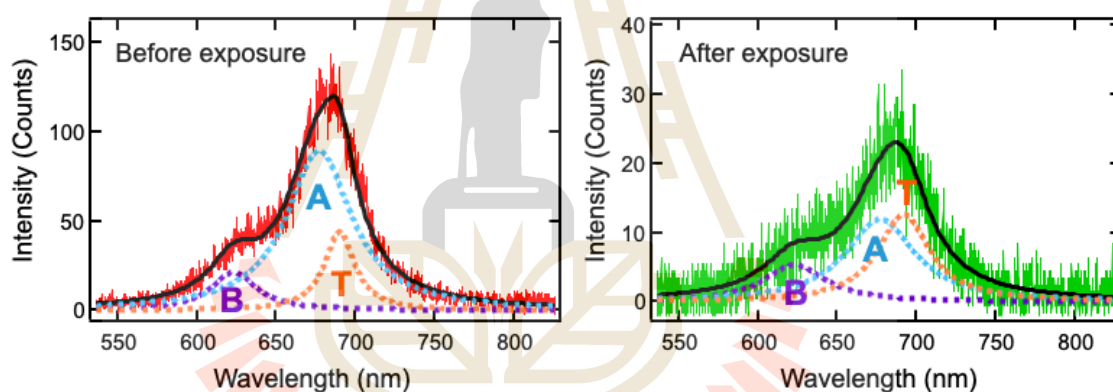


Figure 4.12 Raman peak positions of  $E_2$  and  $A_1$  modes as a function of electron dose.

It is well-known that the formation of S vacancy will reduce molecular symmetry of monolayer  $\text{MoS}_2$  and lead to the change of symmetry assignment in Raman vibrational modes. Here, we observe that after our electron irradiation, the peak positions remained unchanged. Hence, it can be assumed that the electron irradiation did not generate additional S vacancy or structural alteration at the chosen 5 kV acceleration voltage.

### 4.3 Analysis of photoluminescence spectra

Photoluminescent spectroscopy is a powerful optical method used to probe the electronic structure of materials. This technique obtains the photoluminescence spectra that emits from any matter. In this work, we found that the overall PL intensity decreased after exposure to the high-power laser, remained suppressed when kept in  $N_2$  for 10 hours, and recovered after another 10 hours of exposure to ambient condition. Therefore, we will discuss how the physisorption of  $O_2$  can recover the intensity of photoluminescence. To further analyze the effect of the laser exposure, the spectra of the low dose electron irradiated sample before and after exposure to the high-power laser are compared in Figure 4.13.



**Figure 4.13** (Left) The PL spectrum before and after (Right) exposure by high laser power under  $N_2$  fitted with 3 Lorentzian peaks.

Each of the PL spectra is fitted using three Lorentzian functions with peak positions at 623 nm and 677 nm, which correspond to the A exciton and B exciton, and 690 nm, which corresponds to the trion state, respectively. The A and B excitons are the energy difference between the two resonances that results from the spin-orbit coupling in the valence band. After the exposure, while under  $N_2$  atmosphere the integrated A exciton intensity suddenly decreased and the trion intensity increased, while the B exciton remains low. The increase in the trion contribution is consistent with an n-type doping (Sefaattin et al., 2013).

Moreover, the A exciton and trion intensities at 15 minutes and 10 hours under  $N_2$  are unchanged, as shown in Figure 4.14. Hence,  $N_2$  molecules cannot deplete electrons from the monolayer  $MoS_2$ .

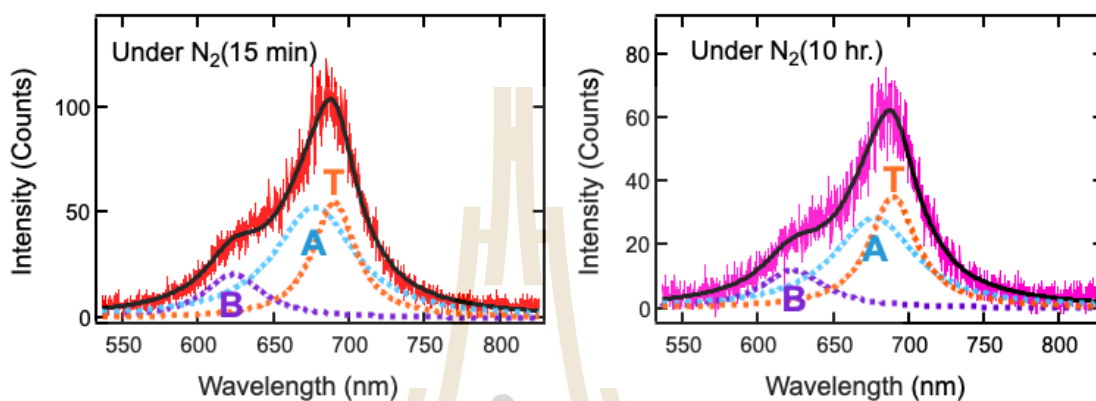


**Figure 4.14** (Left) The PL spectrum at 15 minutes under  $N_2$  fitted with 3 Lorentzian peaks. (Right) The PL spectrum at 10 hours under  $N_2$  is unchanged when compared with 15 minutes.

After storing the sample in the air for 25 minutes, the PL spectrum shows a decrease in the intensity of the trion, which is represented by the purple line in Figure 4.15. Assume the free electron density decreases when  $O_2$  in the ambient environment depletes electrons from the sample.



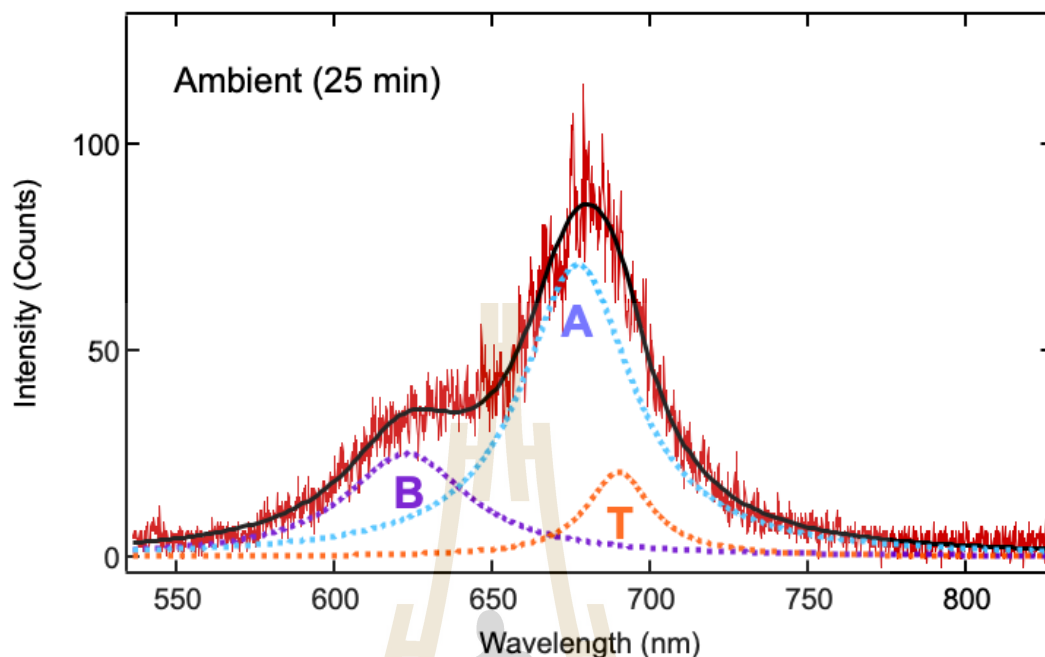


**Figure 4.15** The PL spectrum at 25 minutes under ambient air fitted with 3 Lorentzian peaks, indicating a decrease in the intensity of the trion.

Continuously store the sample in ambient air for 10 hours, the PL intensity can be recovered after high-power laser exposure (Figure 4.6). Then we analyzed the PL spectra that show the PL intensity of the A exciton increasing while the trion decreases, supporting that electrons are being depleted by  $O_2$  molecules present in the ambient air, as shown in Figure 4.16. That means the presence of oxygen molecules adsorbed onto the surface leads to the suppression of the trion.

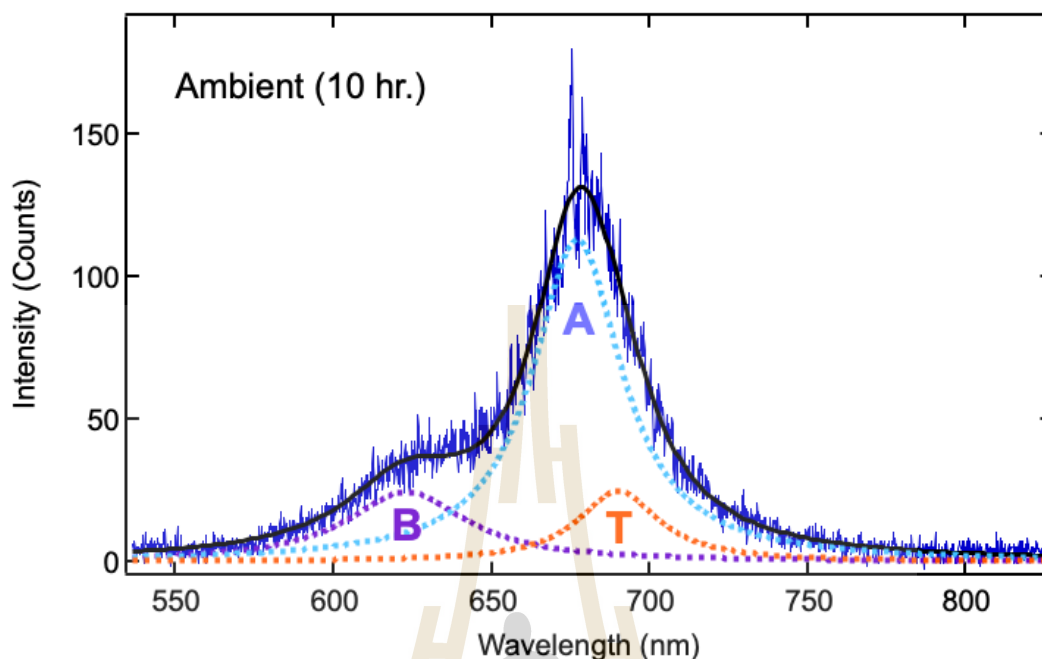


**Figure 4.16** The PL spectrum of MoS<sub>2</sub> was obtained after electron irradiation and exposure to high-power laser for 10 hours in ambient air.

Therefore, we investigated the photoluminescence (PL) behavior of monolayer MoS<sub>2</sub> irradiated under low electron dose conditions in a nitrogen (N<sub>2</sub>) atmosphere for 10 hours, followed by ambient storage for another 10 hours. As shown in Fig. 4.9, the PL intensity remained unchanged in the N<sub>2</sub> atmosphere. In contrast, the PL intensity gradually increased during subsequent exposure to ambient conditions. This result suggests that the significant recovery of PL can be attributed to the physical adsorption of O<sub>2</sub> molecules from the air, which then influences charge transfer from the MoS<sub>2</sub>, depleting the electron of the sample. However, physical adsorption between gas molecules and the surface of MoS<sub>2</sub> is formed by weak Van der Waals force. Since we investigated the PL variation under ambient condition, which consists of 78% N<sub>2</sub> and 22% O<sub>2</sub>, these two types of gas may compete to adsorb on the surface of MoS<sub>2</sub> leading to slow PL recovery.

Normally, the transition probability of the A exciton is typically higher than that of the B exciton due to its lower energy. Consequently, the PL spectrum prominently exhibits the A exciton peak. On other hand, when the electron density is increased, the A exciton transition probability can be suppressed due to the formation of trions, which are bound states of two electrons to a hole that exhibit finite binding energies. We then quantitatively analyzed the PL spectra by deconvoluting the data with three Lorentzian peaks associated with the A exciton, B exciton, and trion, with the peak positions of A and B excitons fixed at 677 nm and 623 nm, respectively. The deconvoluted areas showed no significant change in the exciton and trion intensity during the 10 hours of storage in  $N_2$ , as shown in Figure 4.17. When the sample was re-exposed to ambient atmosphere, the trion intensity gradually decreased, along with the recovery of the A exciton intensity, supporting the assumption that electrons are being depleted by  $O_2$  molecules present in the ambient air.

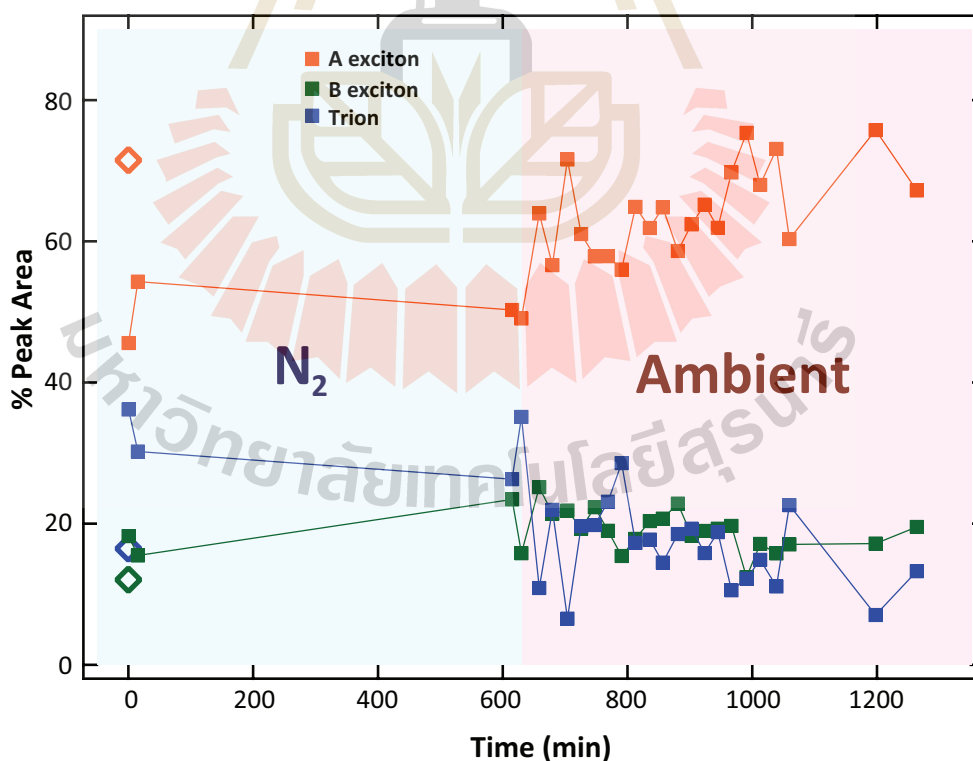


**Figure 4.17** The relative peak area as a function of time under  $N_2$  and ambient conditions. Diamonds indicate the percentages before laser exposure.

Our results have shown that  $O_2$  depletes electrons from the sample, resulting in a decrease in trions and affecting PL recovery in ambient conditions. We conclude the mechanism of this work with the model as shown in Figure 4.18. The monolayer  $MoS_2$  was irradiated with an electron beam on the surface at low accelerating voltage to avoid generating additional defects (Figure 4.18(a)). The PL intensity remained unchanged after electron irradiation, as shown in Figure 4.18(b). We hypothesize that the electron irradiation provided an electronic charge on the sample, which stimulated  $O_2$  adsorption (Figure 4.18(c)). To remove the  $O_2$  adsorbed on the surface, a focused 532-nm laser was used to expose the sample (Figure 4.18(e)). We found that the PL intensity was quenched after laser exposure (Figure 4.18(f)). Our results show that the PL intensity recovers in an ambient environment composed of  $N_2$  and  $O_2$ . Then, we investigated the PL behavior of sample in the  $N_2$  atmosphere for 10 hours followed by an ambient storage for another 10 hours. During the 10 hours of storage in  $N_2$ , the PL intensity decreased and remained unchanged, as shown in Figure 4.19(h). Moreover, the PL spectra at the spot of the white circle in Figure 4.19(h) showed a red shift after the exposure, and the shift remained unchanged while the sample was kept in  $N_2$  (Figure 4.8). After storing in ambient conditions for 10 hours, the PL intensities of the sample exhibited recovery (Figure 4.18(j)). Additionally, the trion intensity gradually decreased, along with the recovery of the A exciton intensity (Figure 4.9). This result suggests that the significant recovery of PL can be attributed to the physical adsorption of  $O_2$  molecules from the air, which then influences charge transfer from the  $MoS_2$ .

Therefore, the adsorption and desorption of  $O_2$  molecules can affect charge transfer from  $MoS_2$ , resulting in changes in the exciton and trion transition probabilities and influencing the PL intensity recovery.

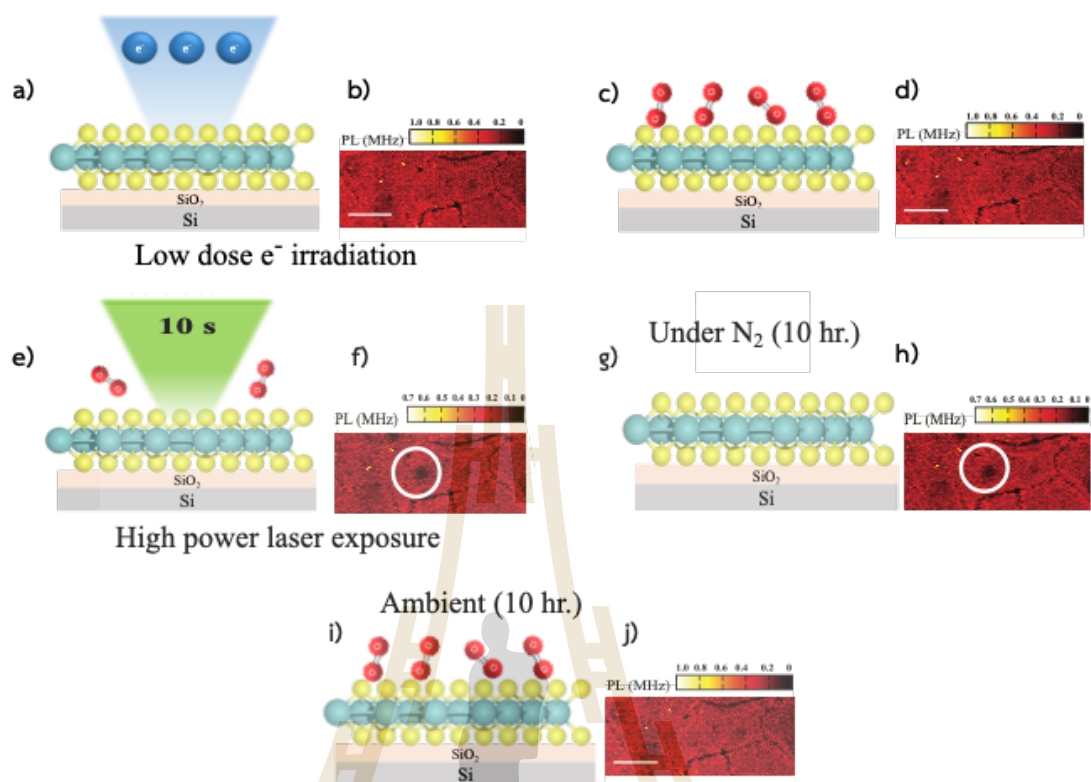


**Figure 4.18** The schematic and confocal images show that O<sub>2</sub> adsorption and desorption on the surface. a) Schematic illustration of electron beam irradiation on monolayer MoS<sub>2</sub> by SEM with 5 kV accelerating voltage and b) confocal PL images. c) Schematic illustration and d) confocal image of O<sub>2</sub> adsorbed on the surface. e) The sample was exposed to 532-nm laser at 14.7 mW under N<sub>2</sub> and f) the quenching area was observed in the white circle. g) Under N<sub>2</sub> for 10 hours, N<sub>2</sub> molecules do not adsorb on the surface and h) the quenching area remained unchanged. i) The oxygen molecules adsorbed on the surface under ambient air and j) the PL intensity recovered.

## CHAPTER V

### CONCLUSION AND FUTURE RESEARCH

#### 5.1 Conclusions

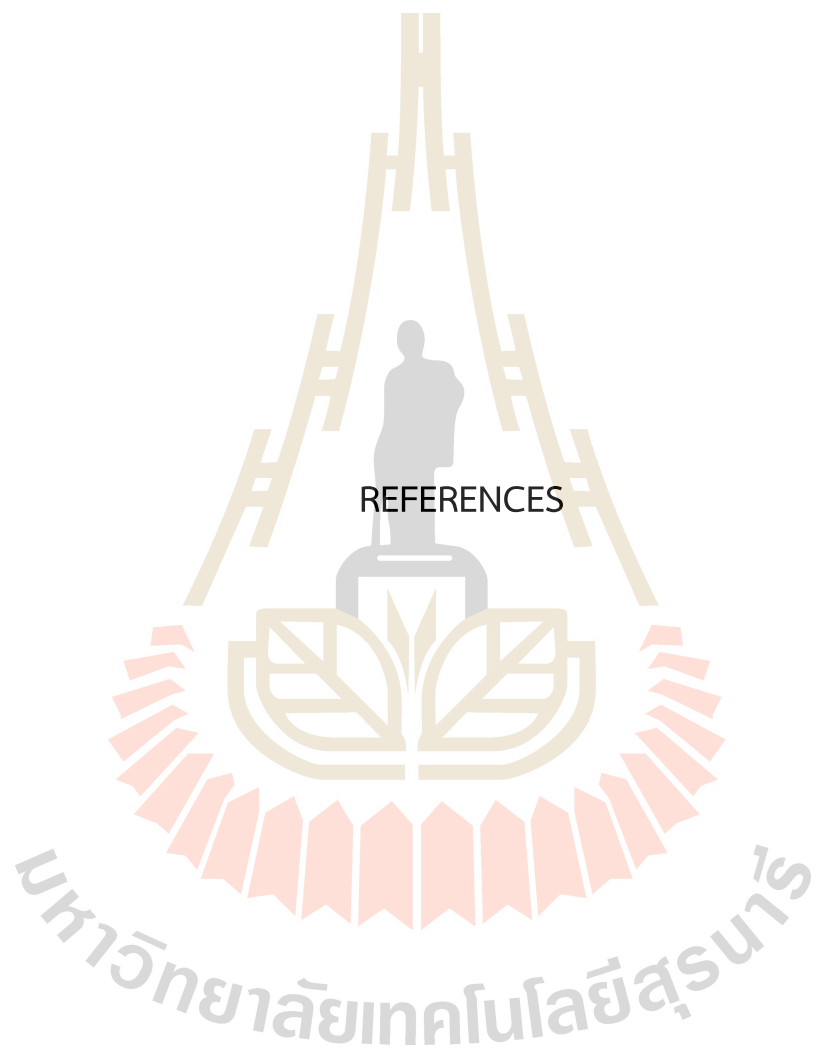
In this thesis, the surface of monolayer MoS<sub>2</sub> was modified by low-energy electron irradiation via SEM. The physical and optical properties were investigated using several spectroscopy techniques to illustrate the effect of low-energy electron irradiation. Upon electron irradiation, we did not observe any shift in the PL spectra that has been previously associated with the generation of vacancies, confirming that the structure remained unchanged after electron irradiation. As the sample was exposed to a high power 532-nm laser, quenching areas were observed. After being stored in ambient conditions for 10 hours, the PL intensities recovered. To identify the gas species associated with the PL recovery mechanism, we investigated the PL behavior of the sample in a nitrogen (N<sub>2</sub>) atmosphere for 10 hours, followed by 10 hours of ambient storage. The PL intensity remained unchanged in the N<sub>2</sub> atmosphere. Furthermore, we observed a red shift in the PL spectrum after laser exposure, which remained unchanged during storage in a nitrogen (N<sub>2</sub>) atmosphere. On the contrary, the spectrum reverted to its original position after subsequent exposure to ambient conditions. However, the PL intensity recovered in ambient conditions, which contain oxygen (O<sub>2</sub>) molecules. Therefore, O<sub>2</sub> is essential for the PL recovery process of the sample. Analysis of deconvoluted spectra revealed a sudden decrease in integrated A exciton intensity, accompanied by an increase in trion intensity, while the B exciton intensity remained relatively unchanged under N<sub>2</sub> atmosphere. Conversely, exposure to ambient conditions for 10 hours led to an increase in A exciton and a decrease in trions, indicating electron depletion from the sample by O<sub>2</sub>.



Therefore, we can conclude that low energy electron irradiation induces a negative charge on the surface of MoS<sub>2</sub>, which stimulates O<sub>2</sub> adsorption. And the adsorption and desorption of O<sub>2</sub> molecules can affect charge transfer from MoS<sub>2</sub>. This process results in changes in the exciton and trion transitions and the recovery of PL intensity.

## 5.2 Improvement and future research

To understand the mechanism within MoS<sub>2</sub> that enables PL intensity recovery after high power exposure, we need to conduct further experiments by varying the dose of electron irradiation. In a previous experimental study with only two doses, we could not explain the threshold dose for the non-recovery of PL intensity. Therefore, we designed to investigate electron irradiation of the sample with 13 electron doses ranging from  $0.1 \times 10^3$  to  $5.3 \times 10^3$   $\mu\text{C}/\text{cm}^2$  (see appendix). If we could further conduct PL intensity recovery experiments in all areas, it would help explain the effects of electron irradiation and photobleaching where PL cannot recover.



## REFERENCES

- Andor, K., Guido, B., Martin, G., Jaroslav, F., Viktor, Z., Neil, D., and Vladimir F. (2015). K-P theory for two-dimensional transition metal dichalcogenide semiconductors. *2D Materials*, 2(2), 022001.
- Berkelbach, T. C., and Reichman, D. R. (2018). Optical and excitonic properties of atomically thin transition-metal dichalcogenides. *Annual Review of Condensed Matter Physics*, 9, 379-396.
- Bhanu, U., Islam, M. R., Tetard, L., and Khondaker, S. I. (2014). Photoluminescence quenching in gold - MoS<sub>2</sub> hybrid nanoflakes. *Scientific Reports*, 4(1), 5575.
- Cho, B., Hahm, M. G., Choi, M., Yoon, J., Kim, A. R., Lee, Y. J., ... and Kim, D. H. (2015). Charge-transfer-based gas sensing using atomic-layer MoS<sub>2</sub>. *Scientific reports*, 5(1), 8052.
- Citrin D.S. (1993). Radiative lifetime of excitons in quantum well: Localization and phase – coherence effect. *Physical review B*, 47(7), 3832.
- Christopher, J. W., Goldberg, B. B., and Swan, A. K. (2017). Long tailed trions in monolayer MoS<sub>2</sub>: Temperature dependent asymmetry and resulting red-shift of trion photoluminescence spectra. *Scientific reports*, 7(1), 14062.
- Coehoorn, R., Haas, C., Fipse, C.J., Groot, R.A., and Wold, A. (1987). Electronic structure of MoSe<sub>2</sub>, MoS<sub>2</sub>, and WSe<sub>2</sub>. I. Band-structure calculations and photoelectron spectroscopy. *Physical review B*, 35(12), 6195.
- Dickinson, R. G., and Pauling, L. (1923). The crystal structure of molybdenite. *Journal of the American Chemical Society*, 45(6), 1466-1471.
- Echeverry, J. P., Urbaszek, B., Amand, T., Marie, X., and Gerber, I. C. (2016). Splitting between bright and dark excitons in transition metal dichalcogenide monolayers. *Physical Review B*, 93(12), 121107.
- Elliott, R.J. (1957). Intensity of Optical Absorption by Excitons. *Physical review*, 108(6), 1384.

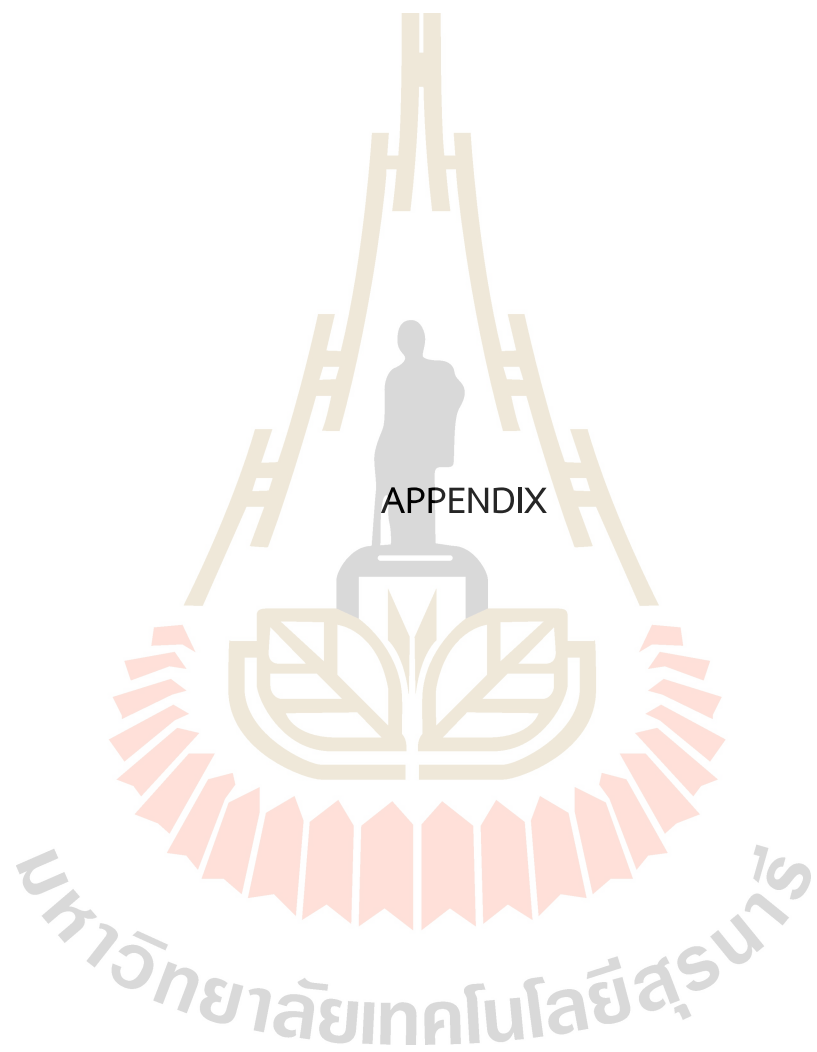
- Ellis, J. K., Lucero, M. J., and Scuseria, G. E. (2011). The indirect to direct band gap transition in multilayered MoS<sub>2</sub> as predicted by screened hybrid density functional theory. *Applied physics letters*, 99(26), 261908.
- Frindt, R. F., and Yoffe, A. D. (1963). Physical properties of layer structures: optical properties and photoconductivity of thin crystals of molybdenum disulphide. *Proceedings of the Royal Society of London. Series A. Mathematical and Physical Sciences*, 273(1352), 69-83.
- Ganatra, R., and Zhang, Q. (2014). Few-layer MoS<sub>2</sub>: a promising layered semiconductor. *ACS nano*, 8(5), 4074-4099
- Geim, A. K., and Grigorieva, I. V. (2013). Van der Waals heterostructures. *Nature*, 499(7459), 419-425.
- Hill, H. M., Rigosi, A. F., Rim, K. T., Flynn, G. W., and Heinz, T. F. (2016). Band alignment in MoS<sub>2</sub>/WS<sub>2</sub> transition metal dichalcogenide heterostructures probed by scanning tunneling microscopy and spectroscopy. *Nano letters*, 16(8), 4831-4837.
- Joensen, P., Frindt, R. F., and Morrison, S. R. (1986). Single-layer MoS<sub>2</sub>. *Materials research bulletin*, 21(4), 457-461.
- Kang, N., Paudel, H. P., Leuenberger, M. N., Tetard, L., and Khondaker, S. I. (2014). Photoluminescence quenching in single-layer MoS<sub>2</sub> via oxygen plasma treatment. *The Journal of Physical Chemistry C*, 118(36), 21258-21263.
- Kautsky, H. (1939). Quenching of luminescence by oxygen. *Trans. Faraday Soc.*, 35, 216-219.
- Ke, J. A., Garaj, S., and Gradecak, S. (2019). Nanopores in 2D MoS<sub>2</sub>: defect-mediated formation and density modulation. *ACS applied materials & interfaces*, 11(29), 26228-26234.
- Komsa, H. P., Kotakoski, J., Kurasch, S., Lehtinen, O., Kaiser, U., and Krasheninnikov, A. V. (2012). Two-dimensional transition metal dichalcogenides under electron irradiation: defect production and doping. *Physical review letters*, 109(3), 035503.
- Kretschmer, S., Lehnert, T., Kaiser, U., and Krasheninnikov, A. V. (2020). Formation of defects in two-dimensional MoS<sub>2</sub> in the transmission electron microscope at

- electron energies below the knock-on threshold: the role of electronic excitations. *Nano letters*, 20(4), 2865-2870.
- Kuc, A., Zibouche, N., and Heine, T. (2011). Influence of quantum confinement on the electronic structure of the transition metal sulfide  $TS_2$ . *Physical review B*, 83(24), 245213.
- Kumar, R. (2020). Chemical Vapor Deposition Grown  $MoS_2$  for Sensing Applications (Doctoral dissertation, Indian Institute of Technology Jodhpur).
- Kumar, R., Zheng, W., Liu, X., Zhang, J., and Kumar, M. (2020).  $MoS_2$  based nanomaterials for room - temperature gas sensors. *Advanced Materials Technologies*, 5(5), 1901062.
- Late, D. J., Huang, Y. K., Liu, B., Acharya, J., Shirodkar, S. N., Luo, J., ... and Rao, C. N. R. (2013). Sensing behavior of atomically thin-layered  $MoS_2$  transistors. *ACS nano*, 7(6), 4879-4891.
- Lee, C., Yan, H., Brus, L. E., Heinz, T. F., Hone, J., and Ryu, S. (2010). Anomalous lattice vibrations of single- and few-layer  $MoS_2$ . *ACS nano*, 4(5), 2695-2700.
- Li, H., Yin, Z., He, Q., Li, H., Huang, X., Lu, G., ... and Zhang, H. (2012). Fabrication of single- and multilayer  $MoS_2$  film-based field-effect transistors for sensing NO at room temperature. *Small*, 8(1), 63-67.
- Lopez-Sanchez, O., Lembke, D., Kayci, M., Radenovic, A., and Kis, A. (2013). Ultrasensitive photodetectors based on monolayer  $MoS_2$ . *Nature Nanotechnology*, 8(7), 497-501.
- Lui, C. H., Frenzel, A. J., Pilon, D. V., Lee, Y. H., Ling, X., Akselrod, G. M., ... and Gedik, N. (2014). Trion-induced negative photoconductivity in monolayer  $MoS_2$ . *Physical review letters*, 113(16), 166801.
- Liu, K., Feng, J., Kis, A., and Radenovic, A. (2014). Atomically thin molybdenum disulfide nanopores with high sensitivity for DNA translocation. *ACS nano*, 8(3), 2504-2511.
- Mak, K. F., Lee, C., Hone, J., Shan, J., and Heinz, T. F. (2010). Atomically thin  $MoS_2$ : a new direct-gap semiconductor. *Physical review letters*, 105(13), 136805.

- Malic, E., Selig, M., Feierabend, M., Brem, S., Christiansen, D., Wendler, F., ... and Berghäuser, G. (2018). Dark excitons in transition metal dichalcogenides. *Physical Review Materials*, 2(1), 014002.
- Mak, K. F., He, K., Lee, C., Lee, G. H., Hone, J., Heinz, T. F., and Shan, J. (2010). Atomically Thin MoS<sub>2</sub>: A New Direct-Gap Semiconductor. *Physical review Letter*, 105(13), 136805.
- Mak, K. F., He, K., Lee, C., Lee, G. H., Hone, J., Heinz, T. F., and Shan, J. (2013). Tightly bound trions in monolayer MoS<sub>2</sub>. *Nature materials*, 12(3), 207-211.
- Molina-Sanchez, A., and Wirtz, L. (2011). Phonons in single-layer and few-layer MoS<sub>2</sub> and WS<sub>2</sub>. *Physical Review B*, 84(15), 155413.
- Mouri, S., Miyauchi, Y., and Matsuda, K. (2013). Tunable photoluminescence of monolayer MoS<sub>2</sub> via chemical doping. *Nano Letters*, 13(12), 5944–5948.
- Najmaei, S., Liu, Z., Zhou, W., Zou, X., Shi, G., Lei, S., ...and Lou, J. (2013). Vapour phase growth and grain boundary structure of molybdenum disulphide atomic layers. *Nature materials*, 12(8), 754-759.
- Nan, H., Wang, Z., Wang, W., Liang, Z., Lu, Y., Chen, Q., ... and Ni, Z. (2014). Strong photoluminescence enhancement of MoS<sub>2</sub> through defect engineering and oxygen bonding. *ACS nano*, 8(6), 5738-5745.
- Oh, H. M., Han, G. H., Kim, H., Bae, J. J., Jeong, M. S., and Lee, Y. H. (2016). Photochemical Reaction in Monolayer MoS<sub>2</sub> via Correlated photoluminescence, Raman spectroscopy, and atomic force microscopy. *ACS Nano*, 10(5), 5230–5236.
- Parkin, W. M., Balan, A., Liang, L., Das, P. M., Lamparski, M., Naylor, C. H., ... and Meunier, V. (2016). Raman shifts in electron-irradiated monolayer MoS<sub>2</sub>, *ACS Nano*, 10, 4134-4142.
- Radisavljevic, B., Radenovic, A., Brivio, J., Giacometti, V., and Kis, A. (2011). Single-layer MoS<sub>2</sub> transistors. *Nature nanotechnology*, 6(3), 147-150.
- Robert, C., Amand, T., Cadiz, F., Lagarde, D., Courtade, E., Manca, M., ... and Marie, X. (2017). Fine structure and lifetime of dark excitons in transition metal dichalcogenide monolayers. *Physical review B*, 96(15), 155423.



- Schedin, F., Geim, A. K., Morozov, S. V., Hill, E. W., Blake, P., Katsnelson, M. I., and Novoselov, K. S. (2007). Detection of individual gas molecules adsorbed on graphene. *Nature materials*, 6(9), 652-655.
- Splendiani, A., Sun, L., Zhang, Y., Li, T., Kim, J., Chim, C. Y., ... and Wang, F. (2010). Emerging photoluminescence in monolayer MoS<sub>2</sub>. *Nano letters*, 10(4), 1271-1275.
- Tongay, S., Suh, J., Ataca, C., Fan, W., Luce, A., Kang, J. S., ... and Wu, J. (2013). Defects activated photoluminescence in two-dimensional semiconductors: interplay between bound, charged and free excitons. *Scientific reports*, 3(1), 2657.
- Yagodkin, D., Greben, K., Eljarrat, A., Kovalchuk, S., Ghorbani-Asl, M., Jain, M., ... and Bolotin, K. I. (2022). Extrinsic localized excitons in patterned 2D semiconductors. *Advanced Functional Materials*, 32(31), 2203060.
- Yin, Z., Li, H., Li, H., Jiang, L., Shi, Y., Sun, Y., ... and Zhang, H. (2012). Single-layer MoS<sub>2</sub> phototransistors. *ACS nano*, 6(1), 74-80.
- Zheng, X., and Zhang, X. (2020). Excitons in Two-Dimensional Materials. In Thirumalain, J., and Pokutnyi, S.P. (Eds.). *Advances in Condensed-Matter and Materials Physics - Rudimentary Research to Topical Technology* (pp. 1-29). doi: 10.5772/intechopen.85564.



APPENDIX

มหาวิทยาลัยเทคโนโลยีสุรนารี

## APPENDIX

### SUPPLEMENTARY RESULTS

We have investigated electron irradiation of the sample with 13 electron doses ranging from  $0.1 \times 10^3$  to  $5.3 \times 10^3 \mu\text{C}/\text{cm}^2$ , as Figure A.1.

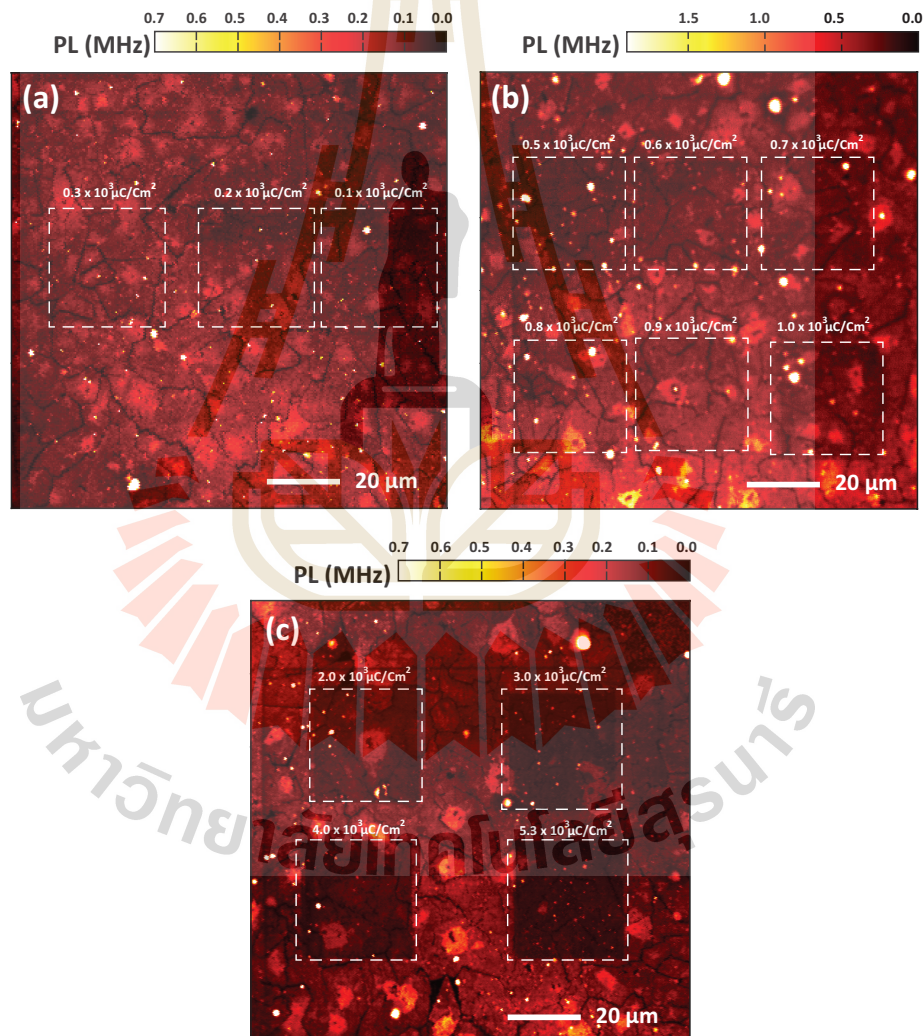


**Figure A.1** Confocal images of monolayer MoS<sub>2</sub> with electron irradiation doses variation, consisting of (a)  $D = 0.1 \times 10^3 \mu\text{C}/\text{cm}^2$ ,  $D = 0.2 \times 10^3 \mu\text{C}/\text{cm}^2$ , and  $D = 0.3 \times 10^3 \mu\text{C}/\text{cm}^2$ , (b)  $D = 0.5 \times 10^3 \mu\text{C}/\text{cm}^2$  up to  $D = 1.0 \times 10^3 \mu\text{C}/\text{cm}^2$ , and (c)  $D = 2.0 \times 10^3 \mu\text{C}/\text{cm}^2$  to  $D = 5.3 \times 10^3 \mu\text{C}/\text{cm}^2$ .

After that, we have analyzed the PL of all the areas post-electron irradiation and showed a decrease in PL intensity, which is a result of photobleaching, as in Figure A.2.

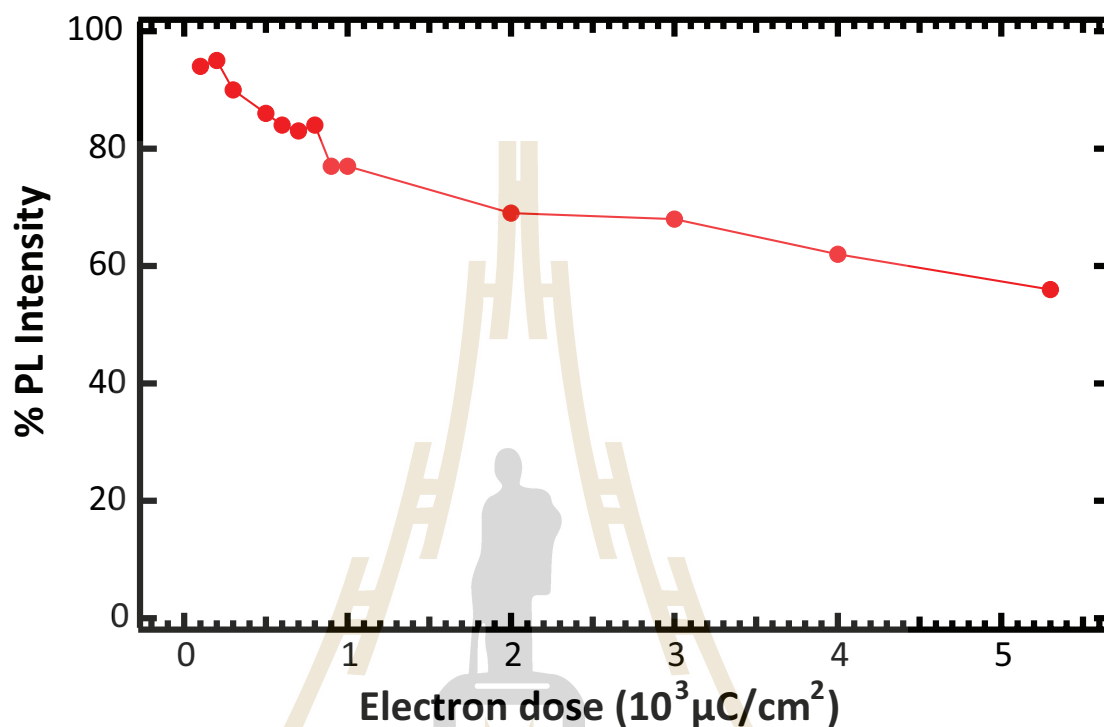


**Figure A.2** The relative PL intensity of the areas exposed by different electron irradiation dose.

Moreover, we observed the PL recovery under ambient conditions for 10 hr. from additional experiments on the lower dose of  $0.2 \times 10^3 \mu\text{C}/\text{cm}^2$  and the intermediate dose  $2.0 \times 10^3 \mu\text{C}/\text{cm}^2$ . Results show the PL recovery with the lower dose of  $0.2 \times 10^3 \mu\text{C}/\text{cm}^2$  (Figure A.3), and with the intermediate dose  $2.0 \times 10^3 \mu\text{C}/\text{cm}^2$ , where photobleaching starts to occur, the PL recovery cannot be observed (Figure A.4).

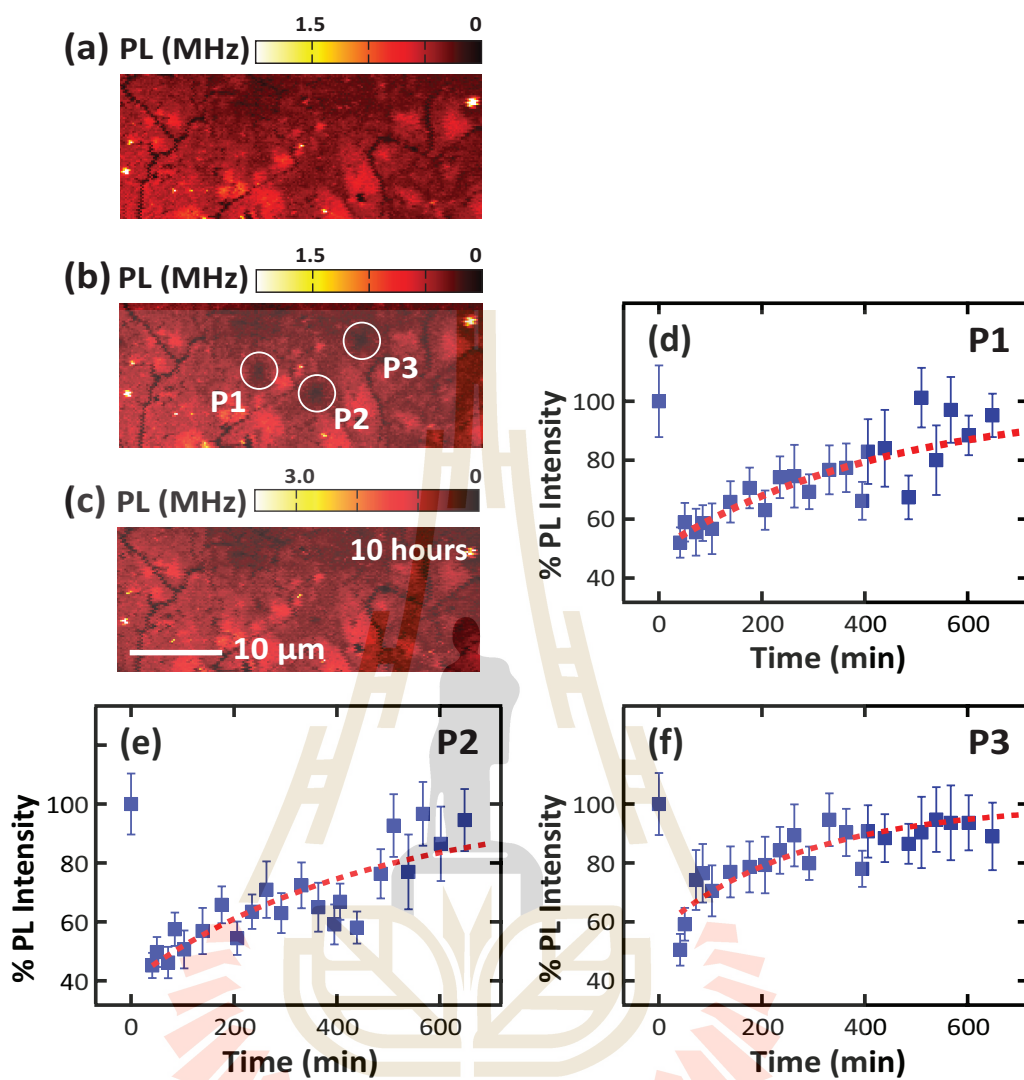


Figure A.3 Relative PL intensity of electron dose irradiation  $D = 0.2 \times 10^3 \mu\text{C}/\text{cm}^2$  areas after high power laser exposure following by ambient atmosphere storage.

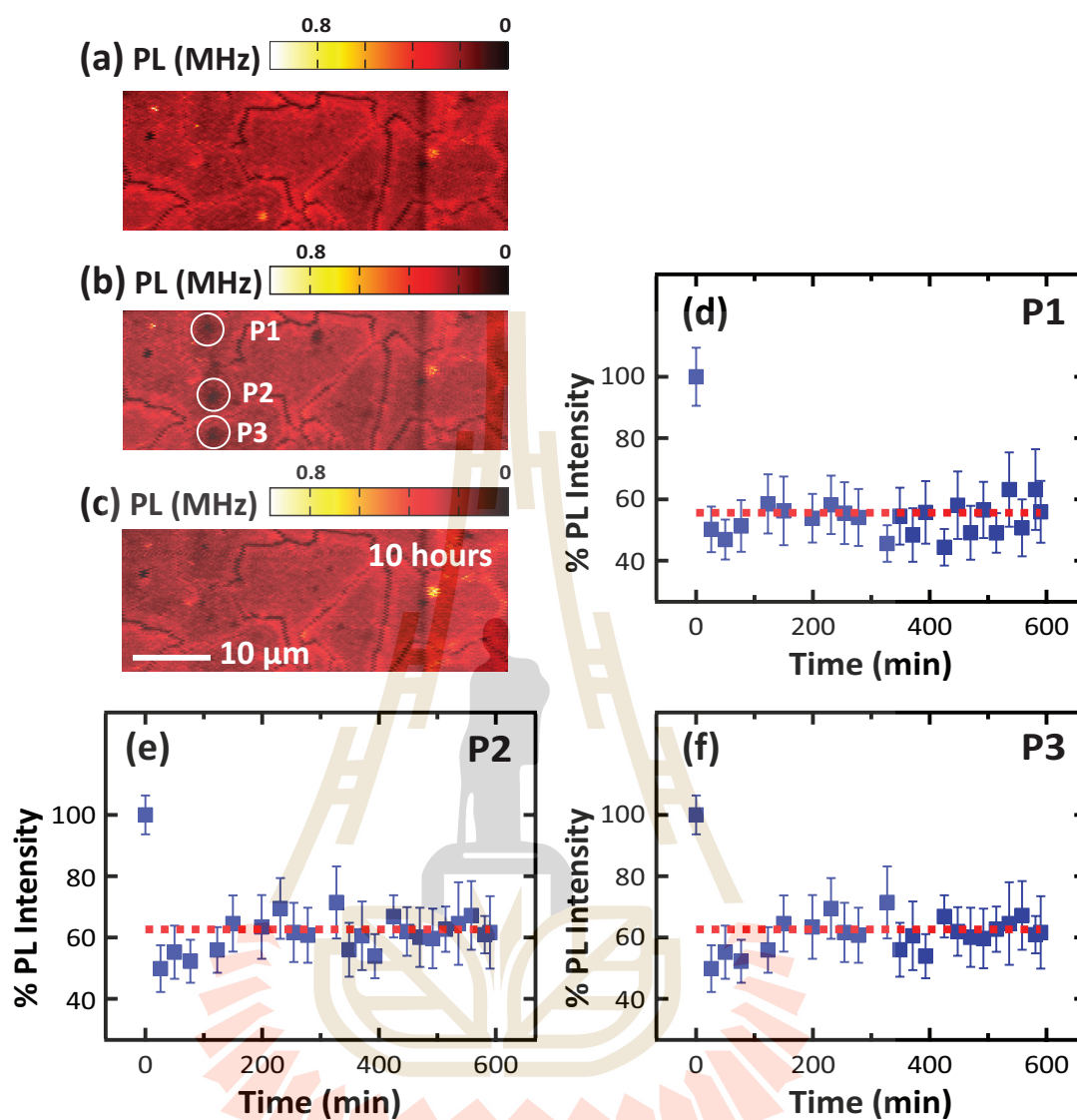


Figure A.4 Relative PL intensity of electron dose irradiation  $D = 2.0 \times 10^3 \mu\text{C}/\text{cm}^2$  areas after high power laser exposure following by ambient atmosphere storage.



## CURRICULUM VITAE

**Name** Ms. Aissara Rasritat

**Date of birth** July 22, 1992

**Place of birth** 7 Mahachaidumri Rd., Talad Sub-district,  
Mueang District, Mahasarakham Province, Thailand.

**Education**

2015-2023 **Doctor of Philosophy (Physics): Ph.D. (Physics)**  
Suranaree University of Technology, Nakhon Ratchasima,  
Thailand.

2011-2014 **Bachelor of Science (Physics): B.Sc. (Physics)**  
Khon Kaen University, Khon Kaen, Thailand.

**Grants and Fellowships** Science Achievement Scholarship of Thailand  
(SAST)

**Publications**

**Rasritat, A.**, Tapakidareekul, M., Saego, K., Meevasana, W., and Sangtawesin, S. (2024). Formation of oxygen protective layer on monolayer MoS<sub>2</sub> via low energy electron irradiation. *RSC Advances*, *14*, 21999.

Polin, S., Laohana, P., Kullapapinyokol, J., Jindata, W., Musikajaroen, S., **Rasritat, A.**, ... and Meevasana, W. (2024). Measurement of the coupling of magnetism with electricity or light irradiation in BiFeO<sub>3</sub> using the Kerr angle. *APL Materials*, *12*, 051104.

Laohana, P., Polin, S., Jindata, W., **Rasritat, A.**, Eknapakul, T., Leusoongnoen, P., Pinitsoontorn, S., Janphuang, P., Saenrang, W., and Meevasana, W. (2022). Large increase in photoinduced conductivity of two-dimensional electron gas at SrTiO<sub>3</sub> surface with BiFeO<sub>3</sub> topping layer. *Applied Physics Letters*, *121*, 241601.

Jindata, W., Hantanasirisakul, K., Eknapakul, T., Denlinger, J. D., Sangphet, S., Chaiyachad, Jaisuk, C., **Rasritat, A.**, and Meevasana, W. (2021). Spectroscopic

signature of negative electronic compressibility from the Ti core level of titanium carbonitride MXene. *Applied Physics Reviews*, 8(2), 021401.

